Point-of-need biosensors for the detection of respiratory biomarkers

Point-of-need biosensors for the detection of respiratory biomarkers

By

Michael Wolfe, B.Sc.

A thesis submitted to the School of Graduate Studies in partial fulfilment of the requirements for the degree Doctor of Philosophy

McMaster University

Doctor of philosophy (2019) McMaster University

(Chemical Biology) Hamilton, Ontario

Title: Point-of-need biosensors for the detection of respiratory biomarkers

Author: Michael Wolfe, B.Sc. (Wilfrid Laurier University)

Supervisor: Dr. John D. Brennan

Number of Pages:

Abstract:

Asthma is a chronic disease affecting over 300 million people worldwide. Airway inflammation is a central feature of asthma. Quantitative sputum cytometry is the most validated method to assess this and to adjust anti-inflammatory therapy, yet it is underutilized due to rigorous processing that requires expensive specialized technicians. To address these limitations, this thesis focuses on the development of several point of need biosensors that rapidly quantify respiratory biomarkers as alternatives to traditional laboratory tests. The project began by developing a paper based sensor for detection of myeloperoxidase (MPO), a neutrophil biomarker. A test was developed using commercially available antibodies, showing direct correlation between the test line colour intensity and total neutrophils. This work was expanded to include a second protein target, eosinophil peroxidase (EPX), for identification of eosinophils. Although the test performed well using neat samples, it failed to identify EPX in clinical sputum samples. Analyzing pre-treatment methods identified that a quick immunoprecipitation technique using protein A/G beads followed by syringe filtration allowed for the device to successfully quantify EPX, eliminating the need for a centrifuge. However, the limited supply of commercial anti-EPX antibodies combined with the need for sample pre-treatment prompted investigation into alternative detection avenues. Nucleic acid aptamers were explored, with aptamer selection for EPX producing several aptamer candidates. Binding affinity and specificity tests were performed, with the T1-5 aptamer emerging. T1-5 was capable of selectively binding EPX over MPO with high affinity. This aptamer was integrated into a simple pull-down assay, capable of detecting EPX with an order of magnitude lower limit of detection than the antibody test. Overall

this work has developed multiple sensors with the potential to overcome the limitations of accessibility to sputum cytometry, rapidly identify the presence and type of airway inflammation, and deliver personalized treatment strategies that not only reduce the global healthcare burden, but also greatly improve a patient's quality of life.

Acknowledgements

I would like to thank my supervisor, Dr. John Brennan, for the opportunity to complete my PhD in your lab. You have provided endless support through critical discussions, funding opportunities, and scientific/ general life advice. Thank you for providing me with the freedom to explore new ideas and the ability to apply my science to real-world problems. Your goofy jokes were a fun bonus.

I would also like to thank my supervisory committee, Dr. Parameswaran Nair and Dr. Yingfu Li, for your advice and criticisms over the years. Your feedback has helped me be more critical of my own work, and I am grateful for all the insight and thoughtful discussions you have both provided.

Thank you to all the Brennanites and fellow colleagues that I have had the pleasure of working with throughout the years. Through coffee dates, group discussions, experimental insights and life chats: I've appreciated it all. I have loved my time here at McMaster, and a large part of that is because of all of you. Thank you to the Mother Liquors graduate student softball team for making sure my liver gets a frequent workout. Furthermore, thank you Tammy Feher for being the angel that you are.

Thank you to my family and friends for their support over the years. You may not have always understood what I was talking about, but you always took the time to listen anyways. Special thanks to my wife Holly for being by my side through all of this. It's been a wild ride, but there's nobody in the world I would have rather done this with.

Table of contents

List of Figures

Figure S2.4 Horizontal layout of the immunochromatographic test strip. The enlarged area depicts an aerial view of the Test (T) line and the Control (C) line.

Figure S2.5 Bland-Altman plot assessing the agreement between the developed LFD and a commercial MPO ELISA. A slight bias (2.80 μg/mL) is observed towards the commercial ELISA.

Figure 3.1: Schematic diagram of the EPX lateral flow test and performance using EPX in buffer and various patient samples. Components of the LFT (A) and sample LFTs using buffer (top) and 10 μg/mL EPX (bottom) (B). T and C refer to the test and control line, respectively. Dose-response curve for EPX present in phosphate buffered saline (C). EPX content was significantly higher in the eosinophilic group when using the gold standard anti-EPX ELISA (D), but the sLFT significantly underreported the EPX content relative to the ELISA (E). Red data points indicate sample had an anti-EPX-Ig OD600 > 1.5. This was further proven using a Bland-Altman plot (F). Blue and red dotted line represent the mean and 95% limits of agreement, respectively. Levels of significance were calculated using the Mann-Whitney or Wilcoxon signed-ranked matched pairs tests. *P < 0.05, **P < 0.01. Bars indicate median while error bars represent interquartile range.

Figure 3.2: Strategy and LFT results of detecting EPX in eosinophilic samples. A simplistic demonstration of the species inside the particular sample and their performance in the LFT (A). Detecting EPX using the bLFT and ELISA shows insignificant differences between detection methods (B). Red data points indicate sample had an anti-EPX-Ig OD600 > 1.5. Correlation between patient's airway EPX content as determined by the bLFT and ELISA (C). Detection of EPX in eosinophilic patients using the LFT showing significant increased detection in sputum supernatants after IP (D). Bland-Altman plot comparing detection of EPX using the bLFT and ELISA (E). Blue and red dotted line representing the mean and 95% limits of agreement, respectively. Comparing EPX in neutrophilic patients and eosinophilic patients using the fLFT shows a significant difference between the two groups (F). Correlation

image of PCR amplified supernatants from various wash cycles. “M” indicates a DNA ladder marker, while the numbers correspond to the wash cycle. (B) Quantified intensity of PCR products. Arrows indicate when the sample was moved to a fresh microcentrifuge tube.

Figure S4.2: Agarose gel image of T1-5 aptamer (3 nM) with increasing amounts of EPX.

Figure S4.3: Dynamic light scattering analysis of the EPX-aptamer complex. Each trace represents an average of three measurements. (A) Intensity of scattered light and (B) volume calculation for EPX and a 1:1 EPX:DNA mixture. The impact of electrical current can be seen with and without a surfactant present, as shown by the (C) intensity and (D) volume calculation.

Figure S4.4: Examining the fluorescent reduction observed when the T1-5 DNA aptamer binds to EPX. The first arrow in all images indicates when protein was added. (A) Comparing the fluorescent intensity when various proteins are added. (B) Fluorescent recovery caused by heating the DNA mixture. The second arrow indicates when the sample was removed and heated at 90 °C. (C) Fluorescent recovery caused by denaturing the DNA-protein complex with 1M urea. The second arrow indicates when urea was added. (D) Fluorescent quenching observed between free fluorescein (no aptamer) and protein.

List of Tables

List of abbreviations

AuNP	Gold nanoparticle
B-cell	B lymphocyte
bLFT	bead lateral flow test
BSA	Bovine serum albumin
COPD	Chronic obstructive pulmonary disease
CV	Coefficient of variance
ECP	Eosinophil cationic protein
EDN	Eosinophil-derived neurotoxin
EMSA	Electrophoretic mobility shift assay
EPX	Eosinophil peroxidase
FeNO	Fractional exhaled nitric oxide
FEV1	Forced expiratory volume in one second
fLFT	filtration lateral flow test
FVC	Forced vital capacity
GOx	Glucose oxidase
IgG	Immunoglobulin G
IL8	Interleukin 8
IP	Immunoprecipitation
LFT	Lateral flow test
LOD	Limit of detection
LAMP	Loop-mediated isothermal amplification
mAb	Monoclonal antibody
MPO	Myeloperoxidase
MRI	Magnetic resonance imaging
NGAL	Neutrophil gelatinase associated lipocalin
pAb	Polyclonal antibody
PO_2	Blood oxygen pressure
PON	Point of need
RAGE	Receptor for advanced glycation endproducts
RCA	Rolling circle amplification
SELEX	Systematic evolution of ligands by exponential enrichment
sLFT	supernatant lateral flow test
ssDNA	single stranded deoxyribonucleic acid
ssRNA	single stranded ribonucleic acid
sIL-5Rα	Serum interleukin 4 receptor alpha
SPR	Surface plasmon resonance
SS aptamer	Structure switching aptamer

Chapter 1 Introduction

1.1 General Overview

With a worldwide prevalence in over 300 million people, asthma remains as one of the most widespread chronic diseases on the planet.[1] In Canada alone this translates into a ~$2.1 billion dollar healthcare burden per annum.[2] Asthma is a chronic, incurable, allergy-driven disease which manifests as difficulty breathing due to constriction and inflammation in the lungs. While majority of asthmatics experience a mild or moderate intensity of the disease, it is estimated that roughly 5 - 10% of patients suffer from severe, refractory asthma.[3,4] This group uses a disproportionate amount of resources and have a higher healthcare burden.[3–5] A major limitation to treating severe asthma is the difficulty in pinpointing the specific asthma endotype of the patient, impeding the use of personalized treatments that would otherwise result in greatly improved patient outcomes.[6–8]

Endotypes are determined by the biological makeup of the lungs, with quantitative sputum cytometry being a well suited laboratory test for identifying and quantifying this.[6,9,10] Both eosinophils and neutrophils are key granulocytes paramount to identifying the asthma subtype and subsequent treatment strategy.[10] While quantitative cytometry has a proven track record, it has yet to emerge as a global technique practiced in most hospitals around the world. Some of the biggest hurdles facing cytometry are the necessity for rigorous sample preparation and highly skilled technical staff essential to analysis.[11] There remains a critical need for simple, portable and affordable sensors capable of identifying the asthma subtype, alleviating the need

for onerous cytometry. In order to develop such tests, the first step is understanding asthma and the basic underlying disease biology.

1.2 Literature Review

1.2.1 Asthma

In theory, the disease is relatively simple: breathing in a noxious substance triggers the immune system to produce cytokines that result in inflammation, while smooth muscle cells constrict resulting in reduced airflow. However, on a biological level the disease is incredibly complex and multifaceted. Numerous cell types are involved, with both external sources (viruses, bacteria, allergens) and innate immune cells responsible for driving the cell-to-cell interactions responsible for asthmatic symptoms. This culminates in a disease that is characterized by heterogenous phenotypes, with a spectrum of patient outcomes and treatment strategies that vary from patient to patient.

Despite the complex nature of the disease, asthma diagnosis is straight forward. Diagnosis is first considered when patients show signs of airway obstruction such as wheezing, chest tightness, tachypnea, and exercise-induced breathing difficulty.[4,12] From there, pulmonary function is then examined via pre- and post-bronchodilator spirometry. Spirometry is a method by which breathing capacity is measured, with the ratio of forced expiratory volume in one second (FEV_1) to forced vital capacity (FVC) painting a picture of airway obstruction.[13] Asthma can manifest as variable airflow obstruction over short periods of time, with the demonstration of improvement in FEV_1 to bronchodilators indicating smooth muscle dysfunction. Despite

inflammation of the airways contributing to this variability, asthma is reversible when adequately treated.

Glucocorticosteroids are the mainstay of treatment for asthma, directed against the inflammatory component, while bronchodilators treat the smooth muscle spasm. However, treatment decisions are often made in clinical practice without measuring the types of inflammation. The past few decades have experienced a shift in treatment strategy, with the understanding that asthma has overlapping features with other respiratory diseases such as chronic obstructive pulmonary disease (COPD) and that the nature of inflammation would be different in various conditions, between patients, and between different episodes of exacerbations of symptoms in the same patient.[14,15] This heterogeneity has resulted in increasing interest in individualized healthcare, with the nature of an individuals' bronchitis being divisible into four main asthma subtypes when assessed via cytometry (Table 1.1). Normal levels are well established, and although the exact values used for subclassification fluctuate slightly from study to study, the overall trends remain the same.[4,6,10,15–17]

Table 1.1: Different asthma subtype classifications.

Classification	**Total cell counts ($\times 10^6$ cells/g)**	**Total Neutrophils (%)**	**Total Eosinophils (%)**
Neutrophilic	≥ 9.7	≥ 64	< 3
Eosinophilic	< 9.7	< 64	≥ 3
Paucigranulocytic	< 9.7	< 64	< 3
Mixed granulocytic	≥ 9.7	≥ 64	≥ 3

All four classes are characterized by their cellular composition, with total cells, neutrophils and eosinophils making up the key analytical markers. By categorizing patients into

their inflammatory subtypes, the heterogenous nature of the disease can be dissected into several small homogeneous groups. Doing so allows each group to be treated with a specific regime, rather than one generic treatment strategy for all four classes.[5–7,10]

Patients with a high total cell count ($\geq 9.7 \times 10^6$ cells/g) and high neutrophil presence, combined with low eosinophil presence are categorized as *Neutrophilic*. This neutrophilia often represents an airway infection, is associated with a poor response to corticosteroid treatment and may be more responsive to antibiotic treatment or anti-neutrophil recruitment therapies.[10,18–20] In contrast, patients with lower cell counts and neutrophilia combined with high eosinophil presence are characterized as *Eosinophilic*. These patients generally have no evidence for bacterial infection, which demonstrates why antibiotics are unlikely to improve their state.[16,21] Instead, they may possess high T-helper 2 cell activity and therefore make up the "Th2 high" or "T2 high" asthmatic endotype. As such, they tend to respond well to corticosteroid treatments and anti-Th2 therapies.[7,9,10,22,23] The past few years have seen approval for a number of biologics (monoclonal antibodies directed against specific Th2 cytokines) to treat severe asthma, particularly those that are associated with eosinophilic inflammation.[24,25] Thus, the ability to specifically identify the type of cells in the airway remains vital to effectively directing these therapies.

Mixed granulocytic patients (both increased neutrophils and eosinophils) usually have more severe symptoms and poorer responses to therapies. They may require treatment with both corticosteroids and with antibiotics.[10] *Paucigranulocytic* patients are interesting in that they have normal levels of both neutrophils and eosinophils, and therefore may not require anti-

inflammatory treatments. While no unique biological markers have been associated with this asthma cohort, they may benefit with novel therapies to try and improve their airway hyper-responsiveness that are largely responsible for their symptoms rather than the inflammatory component.[10,26]

As previously mentioned, the current gold standard for identifying neutrophils and eosinophils involves quantitative sputum cytometry. With normal levels well established, titrating therapies by sputum cytometry has been proven to be extremely effective in managing asthma and COPD.[6–8,27,28] However, this technique is limited in application as low resource areas cannot afford the expensive equipment and specialized technicians required to perform the testing. Point of need (PON) sensors capable of quantifying neutrophils and eosinophils in rapid fashion with minimal processing are desperately needed to overcome these limitations.

1.2.2 Identifying eosinophils

While identifying whole eosinophils is possible, it may be beneficial to identify proteins from these cells as there are many proteins unique to these cells, and they can be present at concentrations much higher than their parent cell. Eosinophils contain cytoplasmic crystalloid granules, termed “secondary granules”, that contain several eosinophil-derived proteins.[29] These granules are composed of a crystalline core made up of major basic protein 1 (MBP-1), surrounded by a cytosolic mixture of eosinophil cationic protein (ECP), eosinophil derived neurotoxin (EDN) and eosinophil peroxidase (EPX).[30] MBP-1 is the smallest of these proteins (14 kDa) and also the most cationic (pI of 11.5) which may partially explain why it is commonly found as a part of eosinophil extracellular traps (EETs).[31] ECP is slightly larger than MBP-1 with

a size ranging from 18 kDa – 21 kDa, and is slightly less cationic (pI of 10.8).[30] It is part of the RNAse A superfamily, and undergoes significant glycosylation that can result in a heterogenous mixture of uniquely decorated ECPs.[32] EDN is unique in that it is much less cationic (pI of 8.9) and also belongs to the RNAse A superfamily.[31] The enzyme is incredibly efficient at digesting invading RNA viruses, with activity comparable to other ribonucleases. It is found at concentrations of approximately 3.3 μg/10^6 eosinophils, roughly 50% lower than ECP and 70% lower than EDN.[33] EPX is the largest of these common granule proteins at a size of 66 – 77 kDa and a pI of 10.8.[30] EPX is the only dimer of the major granule proteins, and is heavily abundant with an average concentration of 12 μg/10^6 eosinophils.[31] EPX is a proficient peroxidase that prefers bromine over chlorine for the production of hypobromous acid (HOBr), and has both pro-inflammatory and anti-inflammatory capabilities.[30,31]

In order to detect granulocytic proteins from eosinophils, degranulation must occur. Degranulation is the direct release of eosinophil granules due to a myriad of causes including exocytosis, piecemeal degranulation, and cytolysis. With these proteins free post-degranulation, biosensors can detect the presence of these targets. A graphene-based sensor was developed by Wang *et al* for detection of ECP, although it required a cyclic voltammetry device that would not be suitable for off-site testing.[34] Unfortunately, the specificity testing did not include any other granulocyte proteins that could result in false positives, so the true usefulness of this device is uncertain. An electrochemical impedance spectroscopy device was developed by Youn *et al* for detection of serum interleukin 5 receptor alpha (sIL-5Rα).[35] The device exhibits great sensitivity

in the low pg/mL range, and was capable of differentiating patients with eosinophilic bronchitis from healthy controls. However, the device is also limited to a laboratory setting.

Enzyme-linked immunosorbent assays (ELISAs) have been developed for several proteins including ECP, EDN, EPX.[36–38] Despite the success of the ELISA technique, it is still limited by long assay times and expensive instrumentation. In addition, one study showed that both ECP and EDN were present in sputum in the absence of eosinophils, suggesting EPX may be the better biomarker to target.[38] With antibodies already developed for EPX it should be fairly straightforward to convert the ELISA into a non-competitive sandwich assay applicable in a LFT format.

1.2.3 Identifying neutrophils

Similar to eosinophils, neutrophils contain several granules with numerous neutrophil-derived proteins that could be used as biomarkers for neutrophil identification. However, unlike eosinophils which house many inflammatory proteins in the secondary granule, many neutrophil proteins are scattered predominately amongst two granules: azurophil (primary) or specific (secondary) granules.[39] Myeloperoxidase (MPO) is the most abundant protein by mass found in neutrophils, and is located in azurophilic granules.[40,41] MPO is a heme-containing homomeric peroxidase with 81% sequence similarity to EPX, although it prefers chlorine over other halides such as bromine for the production of halogenic acids. MPO is a large 146 kDa protein with a pI of 10.[42] Neutrophil elastase is another azurophilic granule protein with protease capabilities, found in both neutrophils and macrophages. Although neutrophil elastase is much smaller than MPO (30 kDa), it exhibits similar cationic capabilities with a pI of 10.5.[43] Cathepsin G is another

protease found in the azurophilic granules. It has a similar size (28.5 kDa) to neutrophil elastase, but is unique in that it is extremely cationic with a pI of 12. It is also different from neutrophil elastase in that it can cleave not only at hydrophobic amino acid sites, but also at basic amino acid sites.[43] Interestingly, the above proteins have been associated with neutrophil extracellular traps (NETs), suggesting they all play a role in the host defense system.[44]

Detecting these biomarkers for neutrophils provides several targets for diagnostic development. A large proteomic study of 40 patients showed a strong correlation between neutrophil defensin and total neutrophil percentage in sputum, suggesting this protein could be an interesting target for sensor development.[45] Human neutrophil lipocalin, also known as neutrophil gelatinase associated lipocalin (NGAL) is found in neutrophilic free granules. While immunoassays and nucleic acid detection platforms exist for this target, they are all limited to being laboratory diagnostics that require expensive instrumentation or several hours to complete.[46,47] The similar situation exists for other neutrophilic proteins such as interleukin 8 (IL-8), receptor for advanced glycation endproducts (RAGE), neutrophil elastase, and MPO.[48–51] Despite originating from neutrophils, detection of these biomarkers as a surrogate identification for sputum neutrophilia has yet to be reliably demonstrated. However, with MPO being the most abundant protein by mass present in neutrophils, it presents an interesting target analyte for neutrophil quantification.

With several potential biomarkers being identified, the next step is transforming traditional lab based diagnostics into portable PON tests. There remains a major need for simple sensing platforms to rapidly identify and quantify the presence of neutrophils and eosinophils in

sputum samples. In order to develop such tests we first must understand the background behind current testing methodologies, and the direction that future diagnostics are headed in.

1.2.4 Biosensors

Worth over 14 billion US dollars, the field of biosensors is a growing area in the scientific community.[52] A biosensor is an analytical device that incorporates biological sensing elements for identification and quantification of an analyte of interest.[53] These devices aim to combine highly specific and sensitive assays with an easy-to-use user interface. Modern biosensors have been developed to utilize numerous design layouts and combine multiple recognition elements to boast a plethora of detection avenues.[53–57] With applications ranging from small molecule trace metal detection to whole-cell bacterial identification, biosensors represent a field with an endless range of applications.

Biosensors help to bridge the gap between traditional analytical laboratories and real-world applications. The low cost and high mobility of biosensors allow for micronization of otherwise cumbersome laboratory equipment for off-site use. This is of particular importance in resource-limited areas that otherwise would not have access to professional labs. An example of this would be in the environmental industry where there is a large demand for identifying the presence of trace toxins in drinking water which range from agricultural pesticides to antibiotic-resistant bacteria. Safe drinking water is paramount for quality of health and biosensors have been developed for numerous toxins because of it.[58–60] Traditional laboratory detection methods require expensive instrumentation, long turnaround times and highly trained professionals for sample analysis.[61] The emergence of biosensors has allowed for these limitations to be reduced.

These devices can be produced using a multitude of analytical techniques and platforms. These techniques all combine a biological sensing element with quantification specific for each method. Some of the most common techniques include surface plasmon resonance (SPR) and sandwich assays (colorimetric, fluorescent, chemiluminescent and electrochemical) while taking the form of microarrays, lateral flow devices, microfluidics and dot-blot assays.[53,61,62] A similar feature of these particular biosensors is the requirement for immobilization onto a solid support. This allows for predefined areas to be created on the device that grant sample separation, washing and multiplexing to occur. Common support materials include glass slides, polypropylene microwells, and cellulose paper as well as numerous chemically modified versions of these same materials. Of these materials, cellulose paper arguably provides the most cost-friendly option for bioassay development.

1.2.5 Bioassay history:

Leland C. Clark is credited as being the "father of biosensors" after he developed the first enzyme electrode for detection of glucose in diabetic patients. Although enzymatic analysis was used as early as the 1930's for different functions, it wasn't until the 1950's and early 60's that Clark was able to transform his oxygen sensor into a reliable bioassay. Frustrated by the poor reproducibility of electrodes at the time, Clark and his group were determined to develop a method for reliable measurement of blood oxygen pressure (PO_2). Initial research was focussed on metal electrode composition and membrane selection, eventually leading to the incorporation of an immobilized enzyme (glucose oxidase, GO_x).[63] This reference provides a good history of his developmental challenges and processes.[64] From here, bioassay development began to

expand. Real-time bioaffinity assays emerged as the knowledge of antibodies grew. Updike and Hicks developed a similar device in the late 60's, followed by other groups later on.[65,66] From here, several groups began to modulate biological enzymes into electrochemical biosensors.[67,68]

During the same time period, paper based diagnostic devices began to emerge. The first paper based analytical device was developed in the mid 1950's by a group in the US for the detection of glucose in urine.[69] This was eventually converted into an immunoassay via the incorporation of antibodies. Since 2013 there has been over 1300 paper based bioassay publications. The evolution of paper has made it an ideal platform for bioassay development. The most recognizable paper based bioassay is likely the household pregnancy lateral flow test (LFT). Renowned for being both user- and cost-friendly, the household pregnancy test is the epitome of simple biosensor development.

1.2.6 Paper as a biosensing platform:

Converting traditional paper-processing technology into biosensor-ready materials requires an understanding of the paper production methodology. The initial processing step requires pulping trees either mechanically or chemically into a mixture rich in free cellulose, resin, fatty acids and possibly lignin depending on the processing.[70] Paper then undergoes a bleaching process (if white paper is desired) followed by the addition of different fillers (buffers, starch, strength-enhancing polymers, ect.). These play an important role in biosensor development as they will influence the surface chemistry of the paper. The end result is a strong paper product largely composed of cellulose.

Paper can function as a great solid support matrix for bioassay development due to several key advantages over other options:

- **i.** Paper is relatively inexpensive when compared to other biosensor supports (e.g. quartz crystal microbalance) and is manufactured worldwide.
- **ii.** Paper can produce low-weight biosensor devices that are easily portable.
- **iii.** Paper can be chemically modified to incorporate a wide variety of functional groups.[71–76]
- **iv.** Recent advances have allowed for simple multiplexing and time-delayed reactions on paper.[77–81]

Cellulose fibres are small hollow "tubes" ~1.5 mm long and 0.02 mm wide. The mixture of these fibers allows for small pores to be formed between adjacent fibres that are enhanced by the intrinsic porosity of the fibre walls. Porosity is determined by a combination of paper properties including thickness (τ, m), base weight (g/m^2), and density (ρ, kg/m^3) combined with drying used in the production method. These factors are important because they have a significant impact on the sensitivity of the developed biosensor. If one assumes an even distribution of porosity and pore sizes amongst the cellulose fibres, increasing the pore size will increase the capillary flow rate. Controlling the flow rate is arguably the most important parameter that dictates the biosensor sensitivity during a LFT assay. This can be explained by analyzing the rate equation (R) for the binding of a capture probe (C) to an analyte of interest (A) (Equation 1):

$$(R) = k[C][A] \tag{1}$$

If the rate of flow is slowed to half the original speed, then the capture probe and the analyte can potentially come into contact for twice as long. This is represented mathematically below:

(2) $$(R) = k[2 \times C][2 \times A] = 4k[C][A]$$

This shows that slowing the flow rate by 50% can increase the effective concentration 4-fold. This sensitivity can be further enhanced by properly positioning the capture probe on the biosensor. As the analyte flows from the sample pad down the LFT it allows the analyte to spread out. As the distance between the solvent front to the origin increases, an exponential decrease in flow rate is observed. Placing the capture probe further down the device away from the sample application zone will allow the capture probe and analyte to interact for a longer period of time due to the decreased flow rate. This further increases the effective concentration of the analyte of interest and is represented below (Figure 1.1).

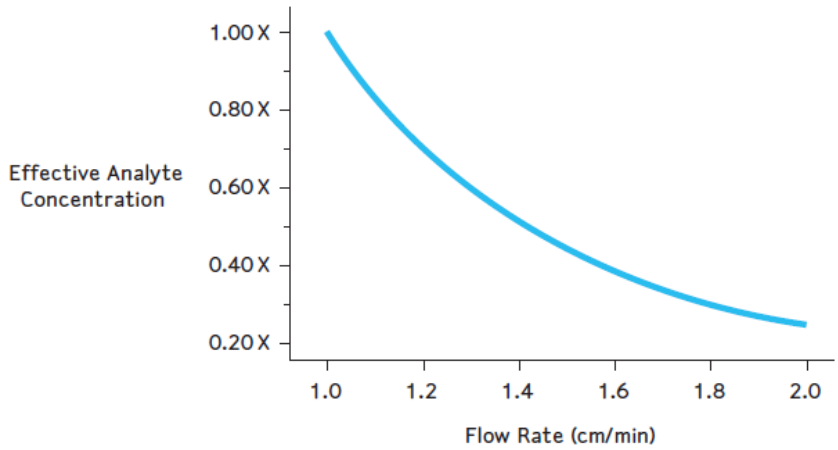

Figure 1.1: Relationship between the flow rate and observable analyte concentration in lateral flow devices. Adapted from Ref. 82.

As mentioned previously, traditional cellulose paper can be modified to incorporate various chemical groups. One of the most common modifications is the conversion of cellulose into cellulose nitrate (commonly known as nitrocellulose). This is done through an esterification

process using nitric acid, resulting in the hydroxyl groups on the cellulose being converted into nitrate groups. This results in the paper having strong protein binding capabilities due to the combination of hydrophobic and electrostatic interactions. This feature combined with rapid flow rates has allowed nitrocellulose to become the dominant membrane used in immunoassay LFT development.

1.2.7 Biorecognition Elements - Antibodies

Antibodies are large immunoglobulin proteins (5 isotypes: IgA, IgD, IgE, IgG, IgM) produced and excreted *in vivo* by B-cell lymphocytes as an immune response to cytokine activation. Produced when the body is infected with foreign molecules including bacteria, viruses and proteins, antibodies are capable of binding directly to the invading compound. This feature has been exploited for biosensor development for over 50 years and is currently the leading recognition probe found in commercial assays.[83] Antibodies are able to bind to target molecules via epitope recognition by their variable region paratope.[84,85]

Developing an antibody specific to the target of interest first requires that the host organism (e.g. mouse, rabbit, goat, ect.) be inoculated with the target cell/protein and an adjuvant to exhibit an immune response. After several rounds of inoculation, the animal is sacrificed and the blood titer is collected and purified. The antibodies are produced by several different B-cells, resulting in a collection of heterogeneous polyclonal antibodies that will potentially recognize different target epitopes on the target antigen. If higher epitope specificity is required then homogenous monoclonal antibodies may be necessary. Creating monoclonal antibodies requires the creation of a hybridoma; fusing a B-cell to a myeloma cell. This ensures that a single variant

antibody is produced that will only recognize a single epitope on the antigen; ideal for sandwich assays.

Despite these features, there are several limitations to the application of antibodies. Antibody production requires non-toxic targets that produce an immune response *in vivo*, limiting the production of antibodies to non-cytotoxic targets. The selection process is both expensive and time-consuming, especially for monoclonal antibodies.[83,84] Even once they are selected, production is expensive and polyclonal antibodies further suffer from batch to batch variations. In addition, antibodies are sensitive to heat and humidity which requires stringent printing and storage conditions during biosensor development.[86] Although satisfactory for traditional sensor development, other biorecognition elements have emerged to provide better sensory options.

1.2.8 Biorecognition Elements - Functional Nucleic Acids:

Functional nucleic acids (FNAs) are nucleic acids designed to carry out a premeditated task, with aptamers being a prime example of FNAs that have been garnering interest over the past several decades. Selected from a random library of ~10^{15} different sequences through a process coined Systematic Evolution of Ligands by EXponential enrichment (SELEX), aptamers are single stranded DNA/RNA (ssDNA/ssRNA) oligonucleotides with high binding affinities for targets of interest . Aptamers are selected through an iterative process of exposing the library to a target (e.g. metal ions, proteins, cell extracts, ect), followed by sequestering bound sequences from unbound sequences. Once the bound sequences are amplified and purified, the process repeats until only a few highly-selective sequences remain. (Figure 1.2).

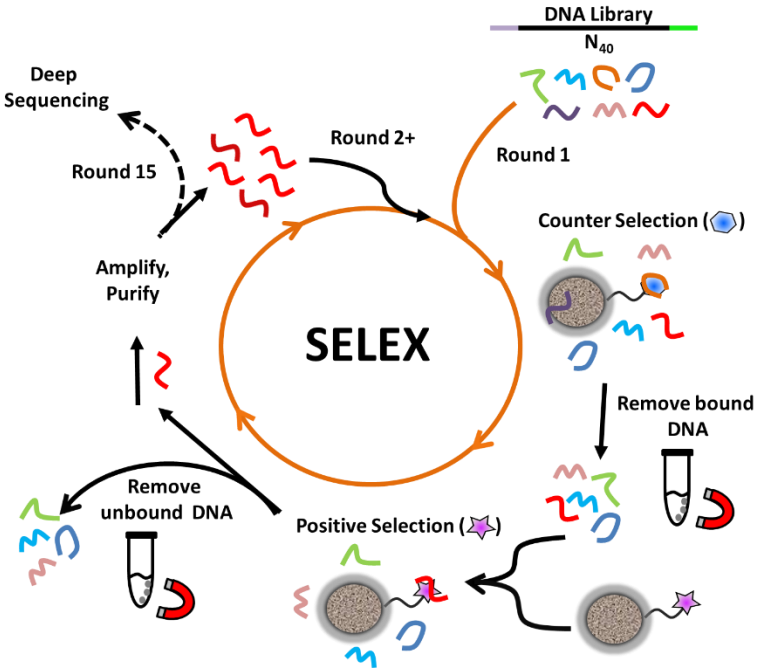

Figure 1.2: Pictorial diagram of a typical aptamer selection.

Functional RNAs were first reported in literature back in the late 1970's and early 1980's, while the term "aptamer" wasn't used until the early 1990's.[87–89] The SELEX process was developed in the early 1990's when multiple groups reported their own versions of the method.[90–92] Aptamers form well-defined three dimensional structures that bind to targets with non-covalent mechanisms similar to antibodies: stacking of aromatic rings, electrostatic interactions, and hydrogen bonding.[93] Aptamers and antibodies have similar binding affinities, typically ranging from pM to µM dissociation constants.[94] In addition, they can exhibit remarkable selectivity as was shown with the theophylline aptamer which is capable of differentiating theophylline from caffeine, a difference of a single methyl group, with 1000 fold selectivity.[95]

Traditional aptamers were designed strictly for binding to the target of interest, allowing them to be interchanged with antibodies in conventional sandwich assays as the capture probe on paper.[96–99] However, aptamers have also been engineered to perform catalytic functions which resulted in the production of ribozymes and DNAzymes. A recently published report from MarketResearch (http://www.marketresearch.com/) estimates that the global field of aptamers was valued at $287 million in 2013, with this value likely to jump to over $2 billion by 2023.[100]

Aptamers are advantageous over antibodies because of several key features. In addition to strong binding affinities, aptamers have a significant cost advantage over their protein-based antibody counterparts. Unlike antibodies, aptamers are produced through chemical synthesis that can be completely automated, resulting in cheap commercial production. In addition to this, many common modifications such as fluorophores or linkers can be incorporated directly into the synthesis, providing precise control over the modification locations. Additionally, aptamers can theoretically be selected via SELEX for any target of interest, while antibodies are limited to non-cytotoxic compounds and analytes that illicit an immune response.

With over 100 publications on aptamer selections in the past five years alone (according to a search in Web of Science), new selection approaches are evolving every year. Traditional SELEX experiments by Tuerk and Gold relied on exposing the RNA library to a protein of interest, then filtering the RNA-protein complex through a nitrocellulose filter.[92] The RNA-protein complex would be caught by the membrane, while nonbinding sequences would be washed away. Since then, various SELEX methods have evolved from immobilizing the target or

the library on magnetic beads, agarose beads, sepharose resins and glass slides to methods that require no immobilization at all such as capillary electrophoresis SELEX [101–105]

Another big change over the years in SELEX techniques have been the rapid improvement in the time required to complete an aptamer selection. Traditional selections typically require 5-15 rounds of selection, resulting in several months to complete the full experiment. However, newer methods can be as fast as a few days or even a single round. Martin *et al* showed that a microarray SELEX experiment can be completed in a single round without the need for PCR amplifications.[106] Arnold *et al* showed that a single round of SELEX was capable of identifying anti-kalikreine-related peptidase 6 (anti-KLK6) aptamers using a microwell plate and increasing concentrations of NaCl washing buffers.[107] A recent report showed that despite these rapid turnaround times, no direct correlation exists between total rounds of selection and binding affinity for the selected aptamers.[108] This is because each round of selection exists simply to reduce the remaining diversity of the random library. Whether you do one round or ten rounds of selection, the strong binding aptamers should still exist in both round populations. However, the diversity of sequences in the 10th round would be expected to be less than that of the one round selection.

Another important aspect of aptamer selection is the composition of the DNA library itself. Most selections have a random domain that typically ranges from 20 – 60 nucleotides, flanked by two primer binding arms necessary for PCR amplification.[104,108] Although these primer binding sites can in theory be part of the active aptamer secondary structure, a bioinformatic analysis into this suggested that the primers are rarely involved in target

binding.[109] Another unique spin on aptamer selections has been incorporating non-normal nucleic acid analogs in the library. One such example is the use of hydrophobic slow off-rate modified aptamers (SOMAmers). These were discovered by Gold *et al* back in 2010 when they added hydrophobic groups onto the nucleoside bases.[110] With DNA/RNA bases being quite hydrophilic, the idea of adding hydrophobic residues was to increase the structural diversity and hydrophobic binding possibilities of the SELEX library, increasing the range of targets that the aptamers could capture. Within this work, they were able to identify SOMAmers for 13 proteins that had failed in previous traditional aptamer selections. To date, this approach has been used to identify SOMAmers for over 3000 protein targets.[104]

1.2.9 Diagnostic methods - lateral flow immunoassay

While antibodies have the ability to detect cells, proteins and small molecules, the size of the target will typically impact the format of LFT used. The two types of sandwich LFT assays are competitive and non-competitive. In a competitive sandwich assay the analyte of interest is immobilized on the test line (typically by covalently linking it to a protein such as BSA). When there is no target analyte in solution, this format results in the labelled antibody being captured on the test line. However, when the target analyte is present in the sample it binds to the labelled antibody before the antibody can bind to the test zone. This results in a decreasing signal proportional to the concentration of target analyte. A visual demonstration is shown in Figure 1.3. This assay format is best suited for small molecules which may not possess the spatial requirements necessary to bind multiple antibodies, and has been used for detection of explosives, growth hormones, and food contaminants.[111–113]

In a non-competitive assay the test line antibody and conjugate labelled antibody both bind unique epitopes on the same target analyte, resulting in a tripartite sandwich complex on the test line. When no target is present, no visible lines appear on the test zone because the sandwich complex cannot be made. As target analyte concentrations increase, this sandwich complex generates a signal proportional to the concentration of the target analyte. This format is better suited for large targets such as proteins or cells.

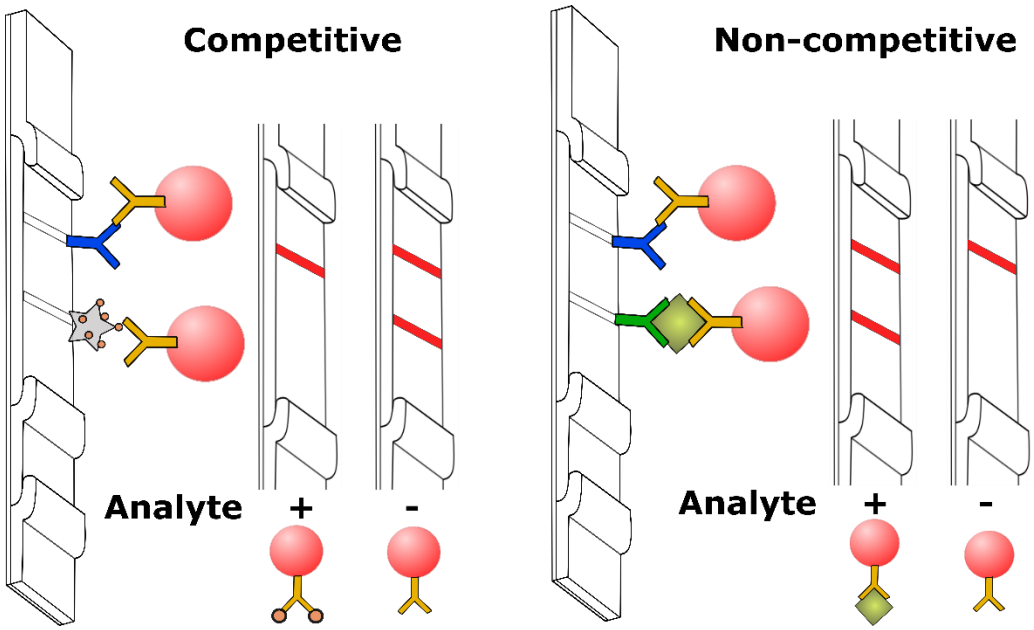

Figure 1.3: General schematic of competitive and non-competitive LFT assays.

In addition to different formats, antibodies have the advantage of being easily immobilized on nitrocellulose membranes. The combination of electrostatic and hydrophobic interactions ensure that simply printing and drying the antibody prevents it from being easily dissociated. In comparison, DNA has little affinity for paper membranes and typically requires some additional immobilization chemistries to prevent it from migrating with the running buffer.[114,115] In addition, antibodies can be conjugated to various detection platforms including

colourimetric nanoparticles, fluorophores, radio labels and enzymes. This allows for a plethora of detection avenues to be tailored to any desired application.

1.2.10 Diagnostic methods - FNA paper based tests

Similar to their protein counterparts, aptamers can also be integrated into similar competitive/non-competitive LFT formats. With regards to paper based diagnostics, aptamers may be preferable to antibodies because of their thermal stability during device fabrication.[86,115] Stability can be further enhanced by entrapping the FNAs in polymeric bioinks such as pullulan, preventing nuclease activity from degrading the oligonucleotide sensors.[116,117] Despite increased stability, the utility of FNAs in paper sensors have been limited because of expensive immobilization chemistries. Unlike antibodies, FNAs are not sufficiently immobilized on paper membranes when printed because the interactions between the membrane and DNA base pairs are too weak.[114] To overcome this limitation, Carrasquilla *et al* developed a paper based sensor using megadalton sized DNA concatemers comprised of repeating aptamer monomers.[115]

Aside from stability, another key advantage to using FNAs instead of antibodies in lateral flow tests is the ability to incorporate signal amplifications, potentially allowing the diagnostic device to achieve ultra-low limits of detection. The two simplest ways to do this are to:

A) Chemically link a sandwich aptamer to an enzyme (analogous to linking an antibody to an enzyme).
B) Utilize the inherent amplification ability of DNA/RNA to self-generate signals via nucleic acid polymerases.

While option A is easy and straightforward, it fails to solve any problems facing immunoassay diagnostics (i.e. protein stability, limit of detection, novel application in a LFT

format, ect). However, option B opens up a plethora of unique detection strategies. Both structure switching aptamers (SS aptamers) and catalytic ribozymes/DNAzymes have the ability to combine target-specific recognition with nucleic acid strand displacement, liberating an oligonucleotide capable of being polymerase-amplified. This liberated oligonucleotide can then be used for isothermal amplification using common techniques such as rolling circle amplification (RCA) or loop-mediated isothermal amplification (LAMP).

This has resulted in several new paper based FNA assays emerging. Hui *et al* combined SS aptamers and RCA in a LFT format to produce peroxidase-mimicking DNA enzymes capable of rapidly detecting both proteins and small molecules.[118] Liu *et al* used RCA on paper to produce the same peroxidase-mimicking DNA enzyme for detection of micro RNAs from breast cancer cells.[119] Toley *et al* created a LFT sensor for rapid detection of methicillin-sensitive *Staphylococcus aureus* after isothermal strand displacement amplification was integrated into a sample preparation step, capable of detecting as few as 10 copies of the gene of interest.[120] Liu *et al* used DNA nanoflowers (produced with RCA) on paper to immobilize anti-*Escherichia coli* DNAzymes capable of fluorescent detection of *E. coli*.[121] Connelly *et al* created a paper based device utilizing LAMP which was capable of detecting a single DNA copy of an *E. coli* gene.[122] Ali *et al* developed a colourimetric LFT sensor for *Helicobacter pylori* (HP) detection by linking a DNAzyme to urease.[123] When HP was present, the DNazyme cleaved an RNA moiety and liberated urease, which was then carried to a detection zone via capillary forces. More examples of FNA paper assays using on-paper amplification/signal generation can be found in the following recent reviews.[124,125]

1.2.11 Current clinical techniques to assess airway inflammation

Aside from quantitative sputum cytometry, another technique practiced in the clinic is to measure fractional exhaled nitric oxide (FeNO). FeNO is produced by nitric oxide synthase enzymes expressed in the airways. The technique is simple and non-invasive, and the American Thoracic Society (ATS) recommends the use of FeNO measurements in determining the likelihood of steroid responsiveness for patients with chronic respiratory symptoms, despite what they called "a low quality of evidence" for the effectiveness of this monitoring method.[126] There are conflicting reports on the effectiveness of FeNO measurements for monitoring sputum eosinophilia, and this technique may be better suited for patients with mild to moderate diseases severity.[127,128] Other biomarkers include serum periostin and blood eosinophils, however they would require an invasive diagnostic as they are found in the blood, and they may not accurately reflect what is going on in the airways.[4]

1.3 Thesis Goals

Despite asthma treatment strategies progressing towards individualized patient therapies, the ability to correctly identify the correct treatment strategy is bottlenecked by tedious quantitative cytometry assays. With no rapid, portable sensors on the market, millions of patients worldwide are forced to visit the few centers practicing sputum cytometry to benefit from the personalized treatments. The research in this thesis aims to address this by developing PON sensors that are capable of detecting biomarkers for eosinophils and neutrophils, while simultaneously alleviating the need for skilled technicians and long assay wait times. The

projects in the subsequent chapters exemplify robust antibody and aptamer sensors capable of approximating key sputum granulocyte concentrations all in under 45 minutes.

To address the need for a simple method to identify neutrophilic bronchitis, the goal was to develop a LFT capable of quantifying MPO as a biomarker for neutrophils, as described in Chapter two. Results showed that detection of MPO alone was sufficient to correctly differentiate neutrophilic bronchitis from healthy patients in majority of the clinical samples tested. The samples required no additional processing to be compatible with the LFT, and results were observable to the naked eye in 15 minutes, much faster than cytology assays. However, the device was only able to identify a single subset of bronchitis, and MPO alone was not a reliable target for identifying eosinophilic bronchitis.

With a sensor capable of quantifying neutrophils, the goal shifted towards developing a similar sensor for quantifying eosinophils, as described in Chapter three. Quantitative sputum cytometry provides information on both these granulocytes, and any LFT hoping to replace this test would require the same caliber of analysis. This began by printing anti-EPX antibodies onto a nitrocellulose membrane to develop a similar lateral flow prototype as the MPO sensor. Although the EPX sensor was able to effectively quantify EPX in neat samples, the developed sensor failed when clinical samples were introduced. In collaboration with researchers at St. Joseph's Healthcare, it was discovered that additional sample-processing would be required due to a high IgG presence in several severe asthma patients. A method for IgG removal was modified for use with the LFT, and then further optimized to eliminate the need for sample centrifugation. Analysis of patient samples showed the new anti-EPX LFT was capable of

differentiating eosinophilic patients from neutrophilic patients. Although the goal of developing a method for eosinophil detection was achieved, this work suggests that a "one size fits all" sensor is not appropriate for all sputum diagnostics. The necessity for sample processing in severe asthmatics prior to using the EPX sensor urges exploration of non-antibody recognition elements for detection of EPX.

With that in mind, Chapter 4 explored DNA aptamers with the goal of developing an alternative detection platform for rapid quantification of EPX. Aptamers are short DNA/RNA oligonucleotides with analogous binding properties to antibodies, without the inherent IgG cross-reactivity problems and batch-to-batch variability experienced by polyclonal antibodies. With no anti-EPX aptamer reported in the literature, aptamer selection was performed to discover one. SELEX was performed, but faced several challenges with the highly cationic EPX. Through trial and error, eventually magnetic bead SELEX was able to produce anti-EPX aptamer candidates. These candidates were screened using an electrophoretic mobility shift assay and fluorescence anisotropy to identify a lead aptamer candidate. The new anti-EPX aptamer was showcased using a simple agarose pull-down assay capable of detecting EPX at ~8-fold lower concentrations than the antibody LFT from Chapter 3, all in under 30 minutes without the aid of specialized technicians.

Finally, Chapter 5 summarizes the major successes and achievements from the above research projects, with a discussion on the future directions for the continuation of this research.

Chapter 2 Development of a functional point-of-need diagnostic for myeloperoxidase detection to identify neutrophilic bronchitis

2.1 Author's Preface

The following chapter was published in the journal *Analyst* under the following citation: Michael G. Wolfe, Qiang Zhang, Christy Hui, Katherine Radford, Parameswaran Nair and John D. Brennan. *Analyst*, 2016, 141(23):6438-6443, DOI: 10.1039/c6an01563h

I was responsible for all experimental design, execution and analysis included in this chapter. Qiang Zhang provided insight into the troubleshooting of the sensor and helped with sample preparations. Christy Hui provided the gold nanoparticles and bioconjugation advice. Katherine Radford and Dr. Nair provided clinical samples and cell staining information. I wrote the first draft of the manuscript. Dr. Nair and Dr. Brennan provided editorial input necessary to generate the final draft of the paper. The article has been reprinted with copyright as per the License to Publish agreement with the Royal Society of Chemistry.

2.2 Abstract

With over 4.8 million Canadians suffering from chronic airway diseases, respiratory exacerbations are currently the leading cause of hospitalization in Canada. In cases of bacterial infection, neutrophil cell density increases from ~10 million cells per gram to over 15 million cells per gram. As sputum is a direct discharge from the primarily affected areas of respiratory

diseases, quantification of granulocytes (including neutrophils) can be used to effectively determine a course of patient treatment. Unfortunately, this quantification is currently limited to labour-intensive and time-consuming cell counts. In the present study, we describe a simple one-step LFT that can semi-quantitatively detect MPO, a biomarker found in neutrophils, in minimally-processed sputum samples. This PON diagnostic device provides positive results observable to the naked eye after 15 minutes. 37 human sputum samples were quantified for MPO using the developed LFT and compared to neutrophil levels quantified through traditional cell counting. A trend between sputum MPO concentration and total neutrophils was observed, suggesting that the LFT has the potential to replace cell counting for neutrophil approximation to aid in directing therapies quickly at the point of need.

2.3 Introduction:

Bronchitis is a central component of airway diseases such as asthma, COPD, chronic cough and bronchiectasis. However, this is infrequently assessed in clinical practice. Quantitative cell counts in sputum provide a reliable and valid measurement of the type and intensity of bronchitis.[129] Neutrophilic bronchitis may indicate infection while eosinophilic bronchitis usually indicates an allergic process. Identification of the type of bronchitis is important as eosinophilic bronchitis is steroid responsive while neutrophilic bronchitis is usually not. There is convincing evidence that treatment strategies guided by sputum cell counts significantly improve clinical outcomes in both asthma and COPD.[6–8] However, these tests are not widely utilized because they are tedious, time consuming, and require a trained technician, adding to the cost of diagnosis.

The ability to detect a biomarker for eosinophils or neutrophils rapidly and cost effectively could overcome many of the limitations inherent to the current cell counting method.

MPO has emerged as a viable biomarker for neutrophils as MPO is the most abundant protein present in this cell (2–5% of cellular dry weight).[40,41] Several commercial kits exist for detecting MPO, but these are generally multi-step assays (such as enzyme-linked immunosorbent assays) and are optimized for use with blood serum. Unfortunately, blood serum MPO levels correlate poorly to pulmonary function and differ significantly from sputum values; therefore these are unreliable for pulmonary diagnostic purposes.[130,131]

The re-emergence of paper-based biosensors provides a viable platform for rapid, robust target identification.[56,58,59,119,132] Such devices have been developed for a variety of clinical markers, including those for liver markers, cancer markers, and infectious disease markers.[133–137] In the case of MPO, there already exist antibodies for this marker, and indeed an antibody-based test for MPO has been produced, but required a three-step addition of reagents in a sequential order, increasing complexity, and was not utilized for direct analysis in sputum.[138] A second group had developed a device for detecting anti-MPO antibodies, however it was designed for blood serum and required a custom optical reader.[139] Herein, we have developed a simple point-of-need LFT for semi-quantitative detection of MPO directly in diluted sputum using anti-human-MPO antibodies printed on nitrocellulose membranes and operated in a lateral flow assay format. We have evaluated the performance of the device using a series of clinical samples and demonstrate that the MPO diagnostic test can enable rapid discrimination of patients with neutrophilic bronchitis from those with eosinophilic airway diseases.

2.4 Results and Discussion

Initial studies focussed on determining the detection limit and linear range of the LFT using pure recombinant MPO (rMPO) samples. To assess these parameters, a standard curve (Figure 2.1) was created by running 100 μL of purified rMPO at various concentrations on the LFT. The test required only 15 minutes for a positive signal and was imaged after 45 minutes to ensure complete colour development. Using the equation produced from the line of best fit (r^2 = 0.98), the test line colour intensity was used to re-quantify the MPO concentrations of the standards used in the curve. The average recovery was calculated to be 105%, showing that the line of best fit is reliable for calculating the MPO concentrations.

The dynamic range of the device was determined to be 0.1–100 μg/mL with a detection limit of 0.25 μg/mL (blank + 3 SD), indicating that the LFT could report over the entire range of clinically relevant MPO concentrations (1 μg /mL – 50 μg/mL).[140–142] This proved to be sensitive enough to provide a detectable signal for all neutrophilic patients and 32/37 total sputum samples analyzed.

Inter-assay (batch-to-batch) variation was calculated by printing 3 different batches of the MPO LFT and testing these with the same solution of 2.5 μg/mL MPO in 1% BSA. All 3 batches were run in triplicate and the test line colour intensity was measured. The average standard deviation was 1.64 corrected intensity units, corresponding to a coefficient of variation (CV) of 11.7%. This suggests that there are minor differences from batch to batch, though not sufficient variation to affect the ability to quantify MPO and determine patient status.

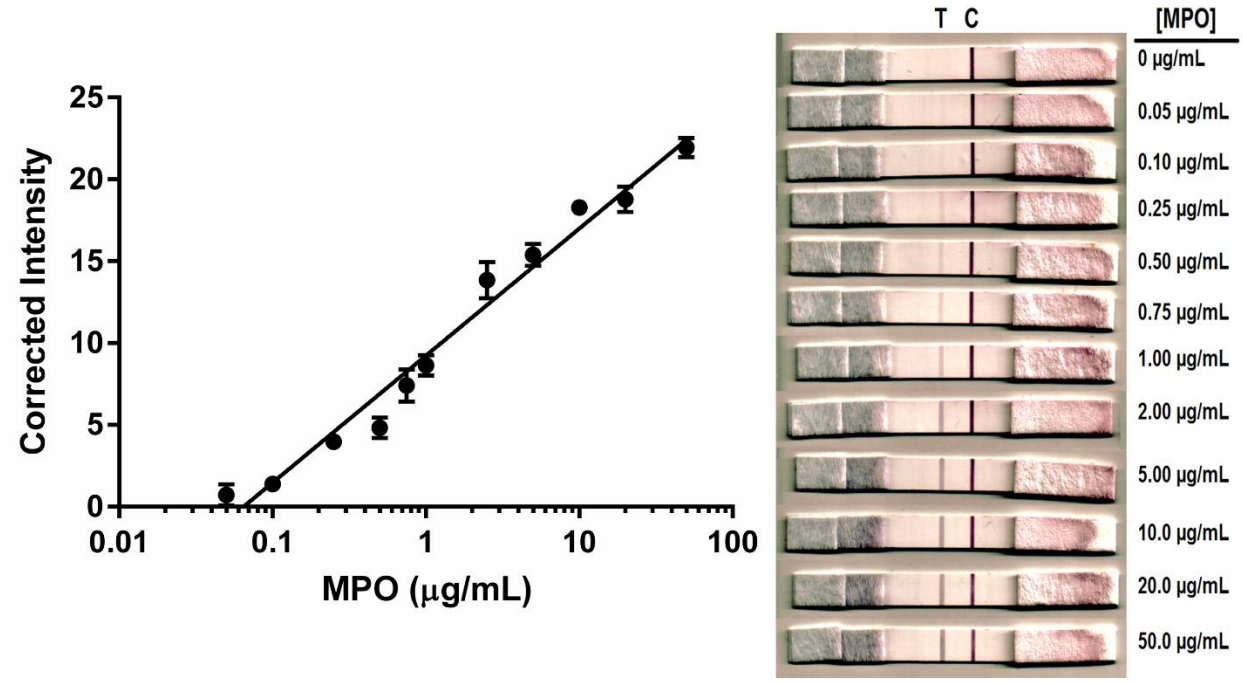

Figure 2.1 Standard curve (left) created by running various concentrations of rMPO on the developed LFT. The LFTs (right) were scanned using a handheld scanner and analyzed using ImageJ software. "T" and "C" are the location of the test line and the control line, respectively.

Intra-assay variation was calculated for 10 different MPO concentrations using the same batch of printed MPO LFTs. All 10 samples were run in triplicate and the test line colour intensity was measured. The average standard deviation was 0.58 corrected intensity units, corresponding to a CV of 6.7%.

Prior to testing sputum samples with the LFT, we first determined the total cell counts from the collection of patient samples. The total cell counts recovered from the sputum samples showed a higher neutrophil presence in the neutrophilic group relative to the other two groups (Figure 2.2i). It was observed that the mean absolute neutrophil counts were higher in the neutrophilic group compared to the healthy group (mean absolute difference, 36×10^6 cells per g

[95% CI, 11–61], P = 0.0067). Compared to the eosinophilic group, the neutrophilic group contained a significantly larger number of neutrophils (mean absolute difference, 38×10^6 cells per g [95% CI, 22–53], P < 0.0001). On the other hand, there was not a significant difference in the total number of neutrophils between the healthy and eosinophilic group (P = 0.26), indicating that the neutrophil count could only discriminate neutrophilic patients from non-neutrophilic patients, but could not further identify eosinophilic patients.

The level of MPO was next quantified in the 37 patient sputum samples with results compared to the cell counting method (Figure 2.2ii). As was observed for the cell count method, the LFT method showed a significant difference between the neutrophilic and eosinophilic groups with regards to quantified MPO concentrations (mean absolute difference, 17 μg/mL [95% CI, 5.1–29], P < 0.01). There was no significant difference between the healthy and eosinophilic group (P = 0.69), in agreement with the cell count results. However, when using the LFT we did not observe as large a difference in the quantified MPO concentrations between the neutrophilic and healthy group relative to cell counts (P = 0.065), primarily owing to the larger spread in values for healthy patients when tested with the LFT relative to cell counts.

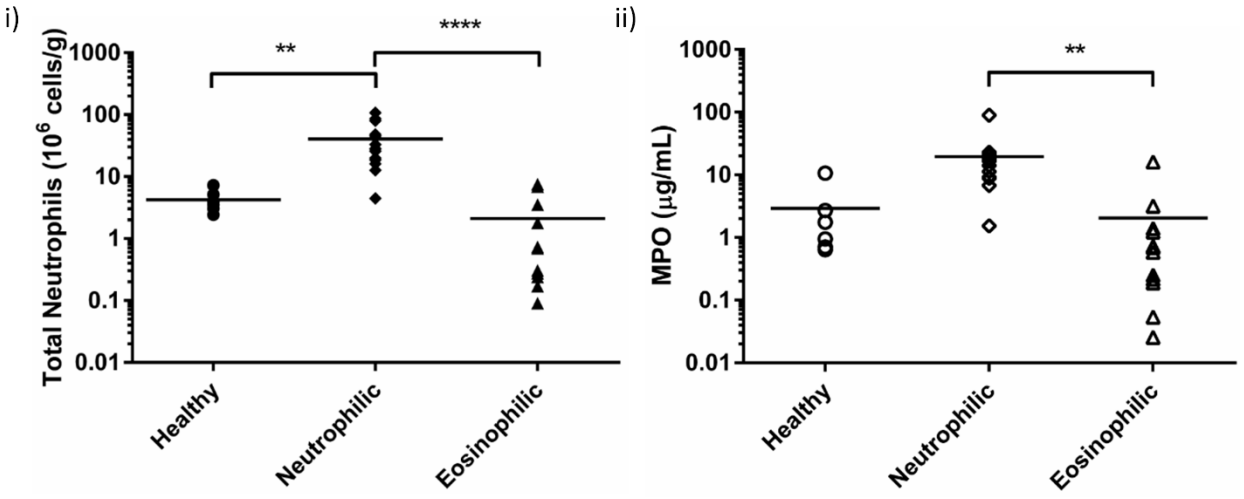

Figure 2.2 (i) Total neutrophil cells for the 37 sputum supernatants used in the study. (ii) MPO quantification for the 37 sputum supernatants. 5 data points are not shown for the eosinophilic group as they were below the quantifiable range of the standard curve. Horizontal bars represent the mean. **P < 0.01, **** = P < 0.0001.

Importantly, one can see that a trend exists between the number of neutrophils (Figure 2.2i) and the concentration of MPO (Figure 2.2ii) in the sputum. This trend indicates that as the total number of neutrophils increases, so does the concentration of MPO. To further demonstrate this, we pooled all the patient data and plotted the concentration of MPO against the total neutrophils (Figure 2.3). As expected, a trend can be observed between the total number of neutrophils per gram of sputum and the concentration of MPO. As such, the data suggests that quantification MPO should be able to differentiate neutrophilic patients from healthy or eosinophilic patients, but not eosinophilic patients from healthy patients. This result can likely be explained by the similar neutrophilic presence between the healthy and eosinophilic patients (Figure 2.2i).

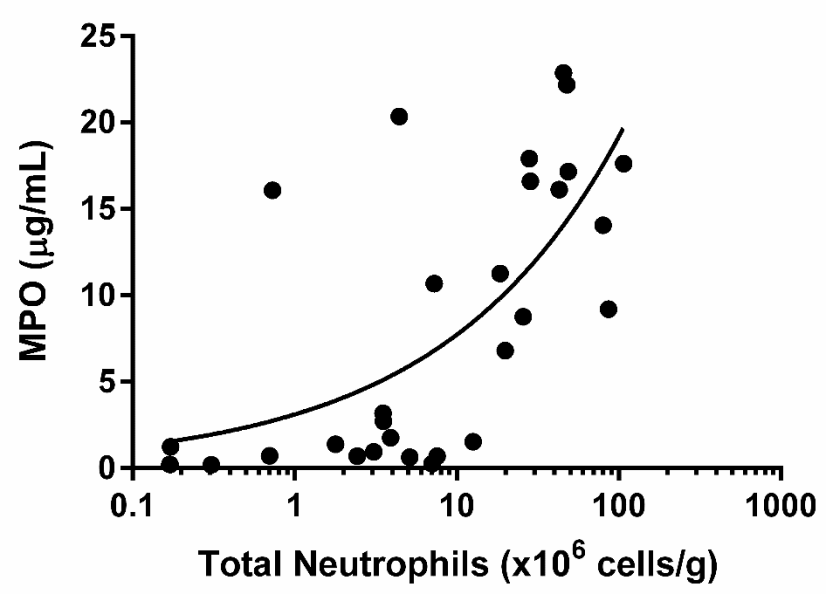

Figure 2.3 Relationship between total neutrophils and MPO concentration for all sputum samples analyzed. One outlier data point was rejected after performing Dixon's Q test.

The validity of the LFT results was examined by comparing the LFT to a commercially available MPO ELISA kit. A total of 20 blind sputum samples were quantified for MPO using both the ELISA and LFT (Figure S2.5). 19 of the 20 samples showed agreement between the two quantification methods, although the commercial ELISA kit reported slightly higher average MPO concentrations relative to the LFT (mean 2.8 µg/mL MPO, 95% CI −7.3–12).

While the LFT was not as sensitive as the commercial solution ELISA (250 ng/mL compared to 63 pg/mL MPO, respectively), it eliminated the necessity for serial sample dilutions. Sputum samples typically required a 1000-fold or 5000-fold dilution to fall within the detectable range of the commercial ELISA kit, greatly increasing the potential for dilution sampling error. The LFT proved to be much more user-friendly (sample filtration and 1:1 dilution followed by sample addition) and delivered visual results in 15 minutes, compared to the

commercial ELISA which required 5 hours and numerous steps to complete. Additionally, the commercial ELISA requires expensive instrumentation for analysis compared to a low-cost handheld scanner for the LFT.

Table 2.1 Results from the MPO LFT analysis of 20 blind patient sputum samples using a cut-off of 2.5 μg/mL MPO.

	Neutrophilic	**Eosinophilic/Healthy**
Total patients, n	10	10
True positives	10	0
False positives	0	3
True negatives	0	7
Fasle negatives	0	0

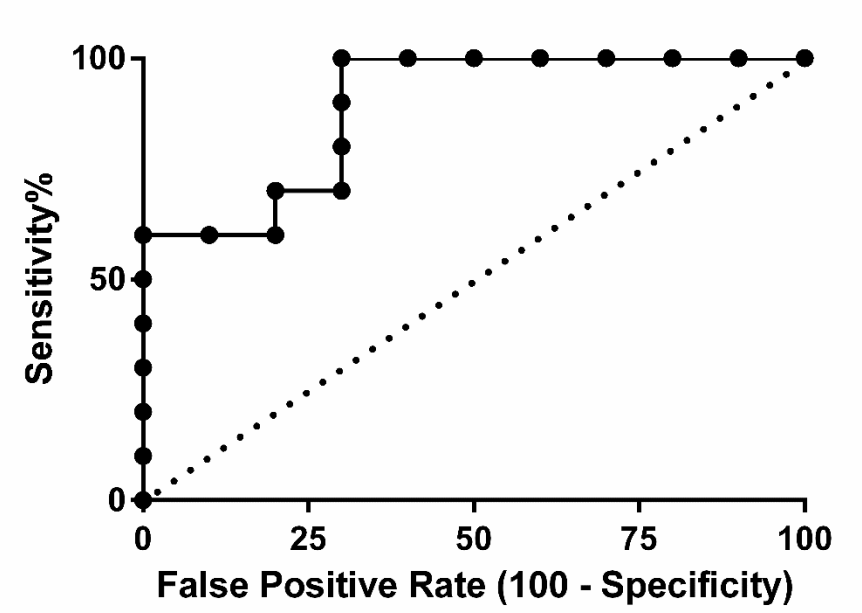

Figure 2.4 Receiver operating characteristic (ROC) plot comparing MPO LFT specificity and sensitivity with blind sputum samples (n = 20).

The accuracy of the developed LFT was examined by analyzing the same 20 blind sputum samples that were used for the validation analysis. Based on previously published clinical MPO values, a cut-off of 2.5 μg/mL MPO was chosen.[140–142] Sputum that had MPO at concentrations greater than or equal to 2.5 μg/mL were considered "positive" for neutrophilic bronchitis, while sputum samples below that threshold were considered "negative". The results (Table 2.1, Figure 2.4) showed the LFT possessed 100% sensitivity (zero false negatives) and a selectivity of 70% (3 false positives).

As expected, the LFT was able to correctly identify all 10 neutrophilic patients. These results show that detecting MPO is a viable method for differentiating neutrophilic bronchitis from eosinophilic bronchitis. However, the results also show that detection of MPO led to 3 false positives (healthy individuals identified as having neutrophilic bronchitis). In a clinical setting however, it is unlikely that stringent differentiation between neutrophilic patients and healthy patients is required, as healthy individuals would not be experiencing severe bronchitis. Differentiation of neutrophilic and eosinophilic bronchitis is more clinically relevant and can be reliably accomplished using the LFT described herein.

2.5 Conclusion

In summary, we have developed a novel point-of-need diagnostic device for the quantification of MPO in patient sputum. The device has a detection range 250 ng/mL–50 μg/mL, relevant for typical patient sputum samples. The test is performed by a single addition of filtered, 1:1 diluted sputum, with colourimetric results observable to the naked eye after 15 minutes. The device allows for approximation of patient neutrophil levels, and possessed 100%

sensitivity when analyzing blind samples. The clinical applications are two-fold: Firstly, rapid detection of normal sputum MPO levels in exacerbations of airway diseases could help physicians exercise proper antibiotic jurisprudence and avoid unnecessary use of antibiotics, given that the threat of emerging antibiotic resistance is one of the biggest health risks in this decade. Secondly, identification of a high MPO level should lead to strategies to identify an infective cause for the exacerbation (usually bacterial) and this would include development of rapid point-of-care tests to detect common respiratory pathogens in respiratory secretions.

Chapter 3 Rapid quantification of sputum eosinophil peroxidase on a lateral flow test strip

3.1 Author's Preface

The following chapter was published in the journal *Allergy* under the following citation: Michael G. Wolfe, Manali Mukherjee, Katherine Radford, John D. Brennan, and Parameswaran Nair. *Allergy*, 2019, 74(6):1176-1178. DOI: 10.1111/all.13711

I was responsible for the LFT experimental design, execution and analysis included in this chapter. I wrote the first draft of the manuscript. Dr. Nair and Manali Mukherjee helped with clinical insight, experimental design for troubleshooting patient samples, and helped with the second manuscript draft. Katherine Radford provided EPX ELISA data, access to clinical samples and cell staining information. Dr. Nair and Dr. Brennan conceived the concept of paper strips for EPX detection and provided editorial input necessary to generate the final draft of the paper. The article has been reprinted with permission from John Wiley and Sons/ RightsLink.

3.2 Abstract

Airway eosinophilia is associated with a number of airway diseases. Titrating therapy by monitoring eosinophil and neutrophil counts has been shown to improve clinical outcomes in asthma and in COPD.[6,8] This can be accomplished by using quantitative sputum cell counts to identify both the type and severity of bronchitis. Despite its proven usefulness in clinical practice, sputum cytometry has not been universally adopted due to the requirements of skilled

technicians, labour-intensive protocols, and incompatibility as a point-of-care test. Our group has recently shown that a rapid, paper-based, LFT for MPO provides a reliable, rapid and potentially cost-effective alternative to cytometry for the identification of neutrophilic bronchitis.[143] Herein we describe a rapid LFT for the detection of EPX, a biomarker that is eosinophil-specific, and demonstrate its utility for testing of processed patient sputum samples.[23,38,144]

3.3 Results and Discussion

A paper based colourimetric LFT was developed using the well-known antibody sandwich format (Figure 3.1A).[145,146] The LFT was calibrated using pure EPX in 1× PBS and 0.1% w/v bovine serum albumin (Figure 3.1B, 3.1C). The LFTs were imaged using a Flip-Pal (#100C) handheld scanner 15 minutes after sample addition (details of method development and materials have been provided in the online repository). The EPX LFT has a linear detection range up to 15 µg/mL and a limit of detection of 500 ng/mL EPX (blank + 3 SD), corresponding to the range that eosinophilic samples are expected to fall into. The LFT signal intensity plateaus above 15 µg/mL EPX likely due to the saturation of the test line antibody. Sputum samples from 15 patients were collected, processed, and counted using routine established methods.[147] The EPX content in the sputum was assessed using a previously established in-house ELISA.[38] As expected, samples from patients with 'controlled' inflammation i.e., sputum eosinophils < 3% of total cells (with a total cell count less than 9.7 million cells)[1] showed lower EPX content compared to the 'eosinophilic' group with > 3% eosinophils (Figure 3.1D, $P = 0.028$).

Using the same sputum supernatants, we then quantified the EPX levels using the LFT (termed "supernatant LFT" or sLFT). To our surprise, we observed a significant decrease in

quantifiable EPX using this technique when compared to the gold standard ELISA (Figure 3.1E, P = 0.004). Furthermore, Bland-Altman analysis shows the sLFT has a bias towards underestimating EPX when compared to the ELISA (Figure 3.1F, mean -6.44; 95% CI -24.79–11.90). Recent work from our group has shown that a third of asthmatics with eosinophilic inflammation have demonstrable titers of anti-EPX IgGs in their sputum, correlating significantly with markers of degranulation.[148] Therefore, we sought to examine (i) if the presence of endogenous autoantibodies to EPX was responsible for reducing EPX detection on the LFTs in eosinophilic samples, and (ii) if removal by an immunoprecipitation (IP) technique would improve detection on the LFTs (the strategy for which has been outlined in Figure 3.2A). The amount of anti-EPX antibodies were quantified using an anti-EPX-IgG ELISA, as previously outlined.[148] Indeed, samples that reported lower values of EPX on the LFT compared to the standard ELISA values, recorded higher titers of anti-EPX IgG, suggesting that the presence of endogenous anti-EPX antibodies could be a confounding factor in EPX capture on LFTs (Figure 3.1E). Therefore, the sputum samples were immunoprecipitated using Protein A/G beads followed by centrifugation to remove any endogenous immunoglobulins (including any anti-EPX IgG), and EPX levels were again quantified using the LFT (termed “bead LFT”, or bLFT). The results show that EPX detection increased after the Ig fraction was removed, and EPX values more closely matched ELISA values (Figure 3.2B, P = 0.85; Figure 3.2C). Eight of the nine patients with eosinophilic inflammation showed increased detection of EPX post-IP using the bLFT (Figure 3.2D, P = 0.008). The Bland-Altman plot comparing the bLFT to the ELISA shows the agreement between the two methods (Figure 3.2E, mean +0.44; 95% CI -

24.79–25.63). The absence of a significant bias and small clustering suggests the two methods produce similar results once the endogenous Igs are removed.

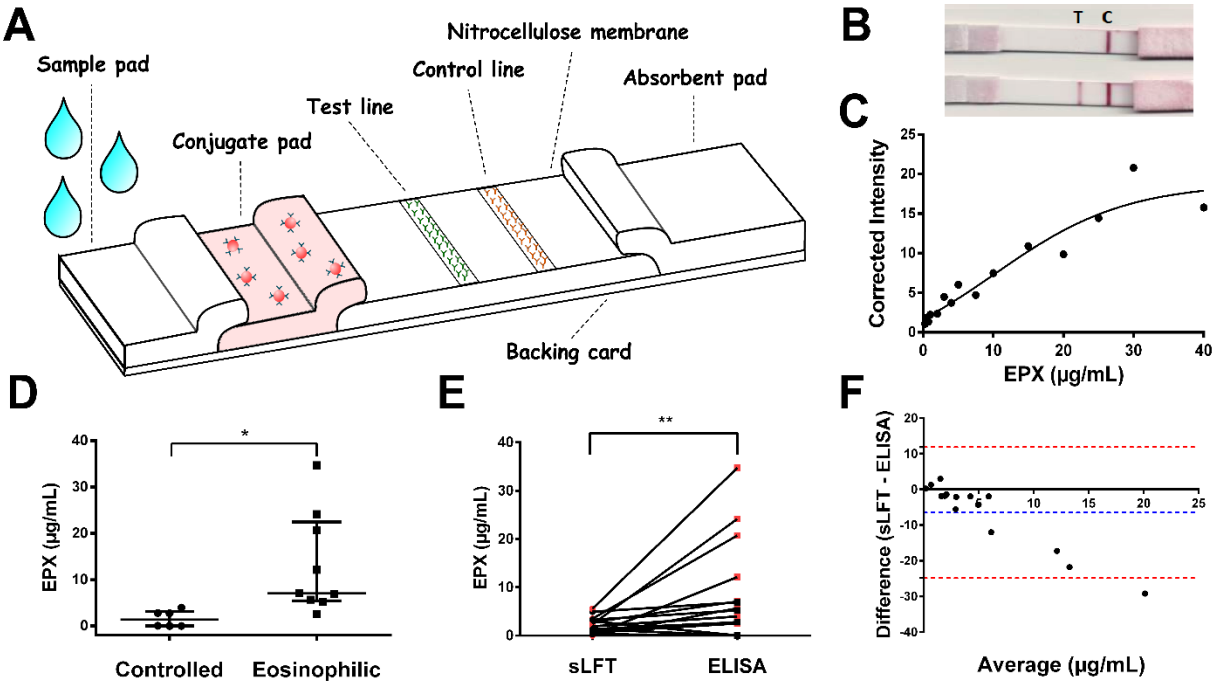

Figure 3.1: Schematic diagram of the EPX lateral flow test and performance using EPX in buffer and various patient samples. Components of the LFT (A) and sample LFTs using buffer (top) and 10 µg/mL EPX (bottom) (B). T and C refer to the test and control line, respectively. Dose-response curve for EPX present in phosphate buffered saline (C). EPX content was significantly higher in the eosinophilic group when using the gold standard anti-EPX ELISA (D), but the sLFT significantly underreported the EPX content relative to the ELISA (E). Red data points indicate sample had an anti-EPX-Ig OD600 > 1.5. This was further proven using a Bland-Altman plot (F). Blue and red dotted line represent the mean and 95% limits of agreement, respectively. Levels of significance were calculated using the Mann-Whitney or Wilcoxon signed-ranked matched pairs tests. *P < 0.05, **P < 0.01. Bars indicate median while error bars represent interquartile range.

To simplify the device into a more convenient point-of-care test, we wanted to remove the centrifugation step of the IP protocol. This was accomplished by incorporating a syringe filtration step to remove the beads (post incubation with the sample) before adding the ‘wash-

through' Ig-free fraction to the LFT (termed "filtration LFT", or fLFT). We collected, processed and counted differential for an additional 25 patient sputa, and quantified the EPX content using both EPX ELISA and fLFT. Though fLFT technique showed a 90% sensitivity and 60% specificity to identify eosinophilia in patient sputa (Figure S3.1) on a receiver operating characteristic curve (ROC), there was an increased detection of EPX in eosinophilic patients (characterized previously by sputum cytology) in comparison to the neutrophilic group (Figure 3.2F, $P = 0.027$), suggesting that this may be a viable method for differentiating the two groups, similar to the results from the ELISA (Figure 3.1D). This agreed with our previous observation[5] that EPX content measured by fLFT is increased in eosinophilic patients with presence of free eosinophil granules ($r=0.7$, $P=0.004$). Indeed, patients whose sputum showed EPX levels ≥ mean (of the eosinophilic group) i.e. 1 μg/mL (on the fLFT), documented 'many free eosinophil granules' in their sputum cytospin slides, and were maintained on inhaled corticosteroid dose ≥ 1000 mcg (fluticasone propionate) and/or daily prednisone.

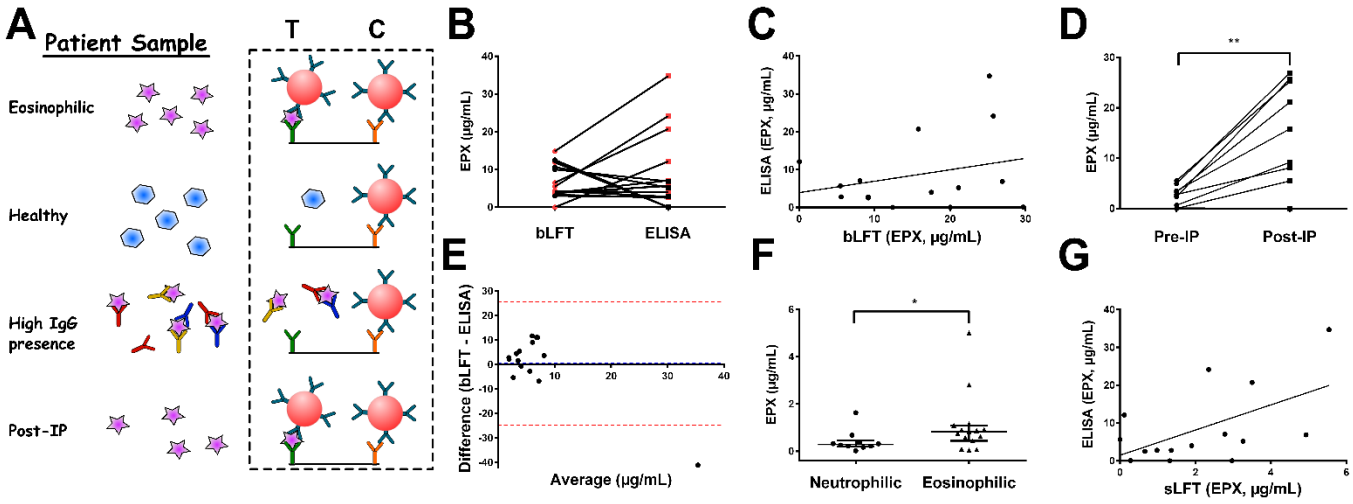

Figure 3.2: Strategy and LFT results of detecting EPX in eosinophilic samples. A simplistic demonstration of the species inside the particular sample and their performance in the LFT (A). Detecting EPX using the bLFT and ELISA shows insignificant differences between detection methods (B). Red data points indicate sample had an anti-EPX-Ig OD600 > 1.5. Correlation between patient's airway EPX content as determined by the bLFT and ELISA (C). Detection of EPX in eosinophilic patients using the LFT showing significant increased detection in sputum supernatants after IP (D). Bland-Altman plot comparing detection of EPX using the bLFT and ELISA (E). Blue and red dotted line representing the mean and 95% limits of agreement, respectively. Comparing EPX in neutrophilic patients and eosinophilic patients using the fLFT shows a significant difference between the two groups (F). Correlation between EPX content when using the sLFT and ELISA (G). Levels of significance were calculated using the Mann-Whitney or Wilcoxon signed-ranked matched pairs tests. *P < 0.05, **P < 0.01. Bars indicate median while error bars represent interquartile range.

3.4 Conclusion

In summary, we have developed a paper-based biosensor that can detect EPX semi-quantitatively in sputum samples with results observable to the naked eye in 15 minutes, without the requirement of skilled labour or laboratory equipment. Although endogenous autoantibodies (as recently observed in the severe eosinophilic asthmatic airways) interfere with the performance of the LFT, this can be overcome via immunoprecipitating the Ig fraction using Protein A/G beads and a syringe filter. While the sputum still needs to be collected and

processed prior to analysis, these modifications not only improve test performance but also allow the device to be applicable in a user-friendly point-of-care format allowing identification of an eosinophilic inflammation, within 45 minutes of sputum induction. The clinical application and performance of this test now needs to be tested in prospective clinical trials.

Chapter 4 Selection of DNA Aptamers for Detection of Eosinophil Peroxidase

4.1 Author's Preface

The following chapter has yet to be published. However, several people have contributed to this work including:

Michael G. Wolfe, M. Monsur Ali, Manali Mukherjee, Katherine Radford, John D. Brennan, and Parameswaran Nair.

I was responsible for the experimental design, execution analysis, and write-up included in this chapter. M. M. Ali provided insight on experimental design and analysis. Dr. Nair and Manali Mukherjee helped with clinical insight and providing sputum samples. Katherine Radford helped provided sputum samples. Michael G. Wolfe, Dr. Nair and Dr. Brennan conceived the concept of the pulldown assay. Dr. Nair and Dr. Brennan provided editorial input on the below manuscript draft.

4.2 Abstract

Eosinophils are granulocytes that play a significant role in the pathogenesis of asthma. Directing patient treatment based on the level of eosinophilia has been shown to be extremely effective in reducing exacerbations and therefore has tremendous potential as a routine hospital test. Herein, we describe the selection and optimization of DNA aptamers that bind to EPX, a protein biomarker unique to eosinophils. 15 rounds of magnetic bead aptamer selection were

performed prior to high throughput DNA sequencing. Sequencing results identified 10 aptamer candidates, which were assessed for EPX binding using a mobility shift assay. This process identified a lead aptamer candidate termed T1-5, possessing low nM affinity with high specificity for EPX over other common sputum proteins. Truncation analysis of T1-5 revealed additional anti-EPX aptamer candidates, although fluorescence anisotropy proved that the full length T1-5 aptamer possessed the best combination of strong affinity with high specificity. This aptamer was then incorporated into a colourimetric pull-down assay, allowing for sensitive detection of EPX in spiked sputum samples. Overall, this work identified the first ever anti-EPX aptamer and showcases a simple assay for sensitive detection of EPX in under an hour.

4.3 Introduction:

With a worldwide prevalence in over 300 million people, asthma remains as one of the most widespread chronic diseases on the planet.[1] In Canada alone this translates into a ~$2.1 billion dollar healthcare burden per annum.[2] One limitation to current clinical asthma management is correctly and rapidly identifying the underlying causes of bronchial inflammation, and personalizing treatment based on those findings. The current gold standard for doing that involves sputum induction followed by histological staining, and has been proven to be extremely effective in managing asthma.[6,7,28] However, this technique is limited in application as low resource areas cannot afford the expensive equipment and trained technicians required to perform the testing. A simpler alternative is to perform high-throughput assays such as ELISAs on surrogate markers for eosinophils, a leucocyte that is highly linked to prevalence and severity in asthma.[7,22,38,149] Unfortunately this is also limited by the long, tedious processing times and

still requires expensive instrumentation. There remains a major need for simple biosensing platforms to rapidly identify and quantify the presence of eosinophils in sputum samples.

The use of EPX has been validated as an ideal biomarker to identify the presence of eosinophils when compared to other surrogate markers.[38] While antibodies have already been developed for this target, recent research has shown that the possibility of an autoimmune response to eosinophil degranulation can result in a high polyclonal IgG presence in the airways.[148] This high IgG presence can complicate rapid antibody lateral flow detection systems, requiring additional sample processing steps.[150] As an alternative, DNA aptamers have garnered a lot of interest as biorecognition elements. Since their discovery in the early 1990's, aptamers have been growing in popularity due to their cheap synthesis, strong stability and simple chemical modifications.[90,92] Using SELEX, aptamers can be identified for a variety of targets.[104] To the best of our knowledge, no nucleic acid aptamer exists for EPX, and the discovery of anti-EPX aptamers has the potential to greatly improve detection platforms for identifying eosinophils.

4.4 Results and Discussion

In the current study, SELEX protocols were carried to identify DNA aptamers with a high affinity for EPX. The first two aptamer selections were performed using a structure-switching aptamer SELEX and membrane SELEX strategy, which have been previously reported for other antigens.[92,151] However, both selections failed to show any obvious DNA enrichment after 10 rounds. The third aptamer selection was a magnetic bead SELEX, with the method illustrated in Figure 4.1. Both EPX and MPO were amide-coupled to separate pools of NHS-

activated magnetic beads. MPO shares considerable sequence homology to EPX and was used as a counter target throughout the SELEX procedure.

The process first began by incubating the DNA library (DNA_L) with the MPO-coated beads to remove any DNA with an affinity for the beads or the counter target MPO. The MPO-coated beads were discarded, and the remaining unbound DNA was used for the positive selection with EPX. To reduce the non-specific electrostatic interactions between the highly cationic EPX and the DNA_L, the selection buffer contained a high concentration of NaCl (1 M) and high buffer pH (pH of 9). The DNA_L was then incubated with the EPX-coated beads, with unbound sequences being removed by thorough washing. PCR amplification of each wash cycle showed that a minimum of 7 washes were required to remove loosely bound DNA and prevent weak-binding sequences from being enriched throughout the selection (Figure S4.1).

The initial magnetic bead selection strategy was termed “T1” and followed a straightforward selection protocol. To further reduce the non-specific affinity of DNA_L to EPX, a second selection (termed “T2”) was performed in parallel that contained a blocking DNA hairpin (DNA_B) in excess of EPX prior to DNA_L addition. The reasoning for this was to ensure any non-specific DNA-binding sites on EPX were blocked prior to exposure to the DNA_L. PCR amplification of DNA_B showed no unintended amplification of this sequence during the DNA_L amplification process.

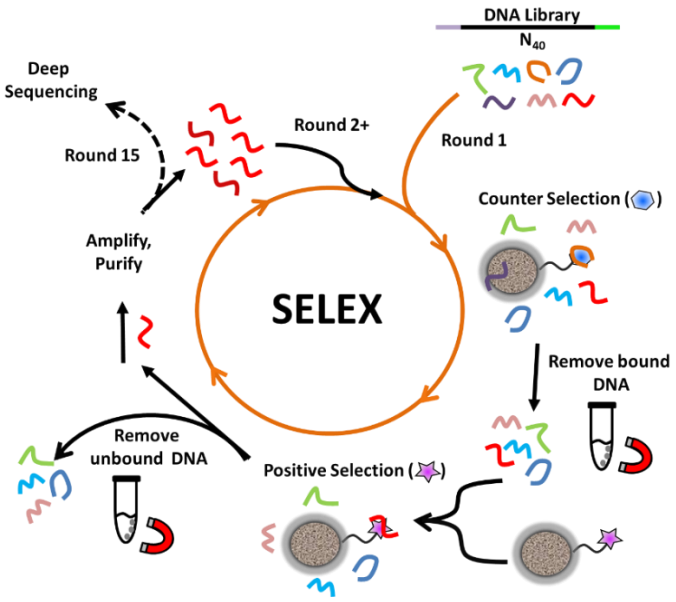

Figure 4.1: Schematic illustration of the SELEX procedure using EPX covalently linked to magnetic beads.

After 15 rounds of selection, the final DNA elution was performed using free EPX instead of heat to ensure the sequences could bind the free version of EPX. Eluted sequences were PCR amplified and sent for deep sequencing, with results indicating an enrichment of aptamer sequences. It is interesting to note that between the two selection types (T1 and T2), only a single sequence was shared amongst the top 10 populated sequences. This shows that the addition of the DNA_B in the T2 selection resulted in a different evolution of sequences. It was also interesting to note that many of the enriched sequences were heavily guanine based, with some sequences being comprised of 60% guanine. It could be that the presence of potassium combined with the buffer's high ionic strength pressured the DNA_L to form stable tertiary structures during the selection such as G-quadruplexes, which are known to have a high affinity for proteins.[152]

To screen these aptamer candidates, an electrophoretic mobility shift assay (EMSA) was performed using five of the top sequences from both the T1 and T2 selections (Figure 4.2, Table S4.4). Interestingly, the aptamer-EPX complex could not directly be quantified in the EMSA as the bound complex did not migrate through the gel (Figure S4.2). Despite this, the fraction of bound aptamer could still be calculated by subtracting the intensity produced by unbound aptamer from a control well. The binding of all 10 aptamers were quantified, with the best aptamer T1-5 possessing a K_d of 9.2 ± 1.6 nM. It was interesting to note that the addition of DNA_B to this assay resulted in no noticeable reduction in binding affinity between T1-5 and EPX, despite being well in excess (100 fold greater than T1-5). This suggests that the binding is specific, otherwise DNA_B would compete with T1-5 for the same non-specific binding sites on EPX, resulting in reduced EPX/T1-5 complexes.

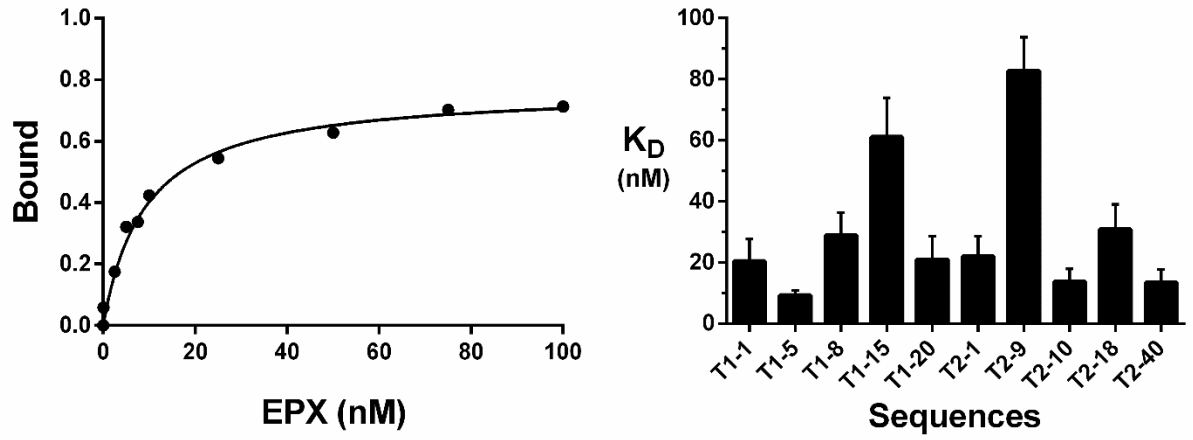

Figure 4.2: Analysis of EPX aptamers using an electrophoretic mobility shift assay. (A) Binding curve for the interaction between T1-5 and EPX. (B) Calculated dissociation constants (K_d) for the full length screened aptamers. Error bars represent the standard error in the calculated K_d, as determined by the GraphPad Prism software.

To investigate the poor mobility of the EPX/T1-5 complex, dynamic light scattering (DLS) on the T1-5/EPX complex was performed. Results showed that the T1-5/EPX complexes were small enough (< 10 nm) to be able to enter into the pores of the agarose gel (Figure S4.3A, S4.3B).[153] However, running current through the gel leads to the precipitation of the protein/DNA complexes (Figure S4.3C, S4.3D). Addition of a surfactant slightly helped reduce the amount of aggregated complexes, but it had no impact on the EMSA gels.

With initial aptamer screening complete, aptamer truncation and mutation was performed. The T1-5 aptamer was truncated by removing various DNA segments, then affinity for EPX was assessed using the EMSA (DNA sequences in Table S4.1). Results showed the same protein precipitation issue that was experienced with the full length constructs, but binding was still able to be measured by quantifying the unbound DNA band. Results showed that removing the 3' stem loop of T1-5 significantly reduced binding affinity (T1-5.A), while deletions located in the middle of the sequence had a lesser effect on EPX binding capabilities (T1-5.B, T1-5.C). Interestingly, switching several guanosine residues for adenosine residues also resulted in a significant reduction in EPX binding (T1-5.D). These mutations likely result in the inability to form a stable G-quadruplex, a structure common in many protein binding aptamers.[152,154] Overall, the T1-5.C aptamer showed the highest binding affinity via the EMSA experiment, with the predicted structure comparison to T1-5 shown below (Figure 4.3A, 4.3B).[155]

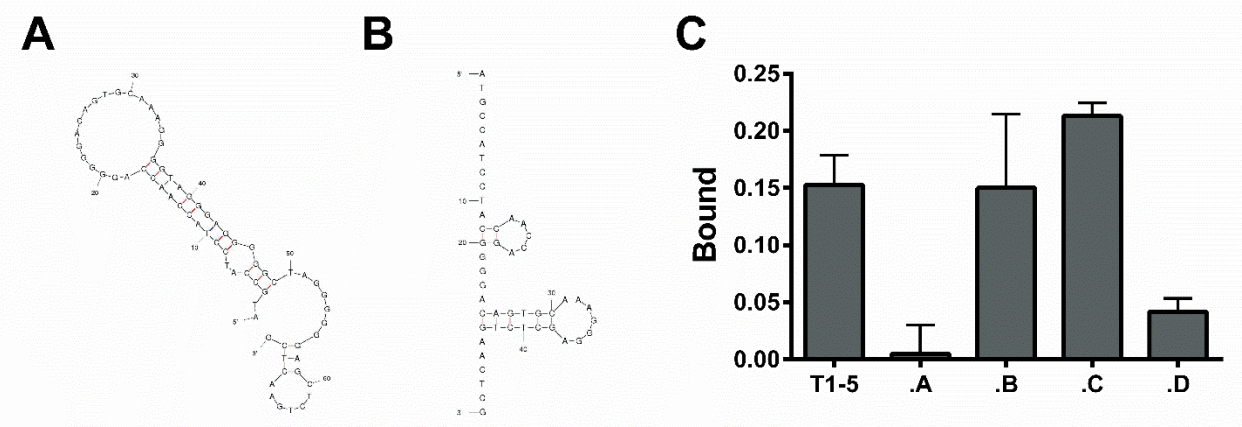

Figure 4.3: Analysis of truncated EPX aptamers using an electrophoretic mobility shift assay (EMSA). (A) Predicted T1-5 and (B) T1-5.C aptamer structures.[155] (C) Screening truncated variants of T1-5 using the EMSA. Fraction of bound aptamer (3 nM) with EPX (5 nM).

To further confirm the binding between T1-5.C and EPX, fluorescence anisotropy was performed. Interestingly, no anisotropy could be observed for the binding between EPX and either T1-5 or T1-5.C when using 1× SB (Figure 4.4A, 4.4C). Diluting the buffer to 0.5× SB resulted in an increase in anisotropy, with a calculated K_d of 36.6 ± 4.8 nM for the T1-5 aptamer (Figure 4.4A). We hypothesize that the lower salt concentration of the 0.5× SB likely results in reduced masking of charges on EPX, increasing the affinity between EPX and T1-5. However, it was interesting to observe that the T1-5.C aptamer had very little binding affinity for EPX despite the reduced salt concentrations. To further investigate the importance of the binding conditions, the interaction between EPX and T1-5 or T1-5.C was observed in PBS. As expected, binding affinity was further increased in the lower salt environment with a K_d of 4.3 ± 1.6 nM for T1-5 and 4.8 ± 2.0 nM for T1-5.C (Figure 4.4A, 4.4C). However, the low ionic strength buffer also resulted in increased MPO affinity for both T1-5 and T1-5.C (Figure 4.4B, 4.4D). Based on

these results, the T1-5 aptamer was used for all future experiments with 0.5× SB as it provides the best combination of high affinity and specificity.

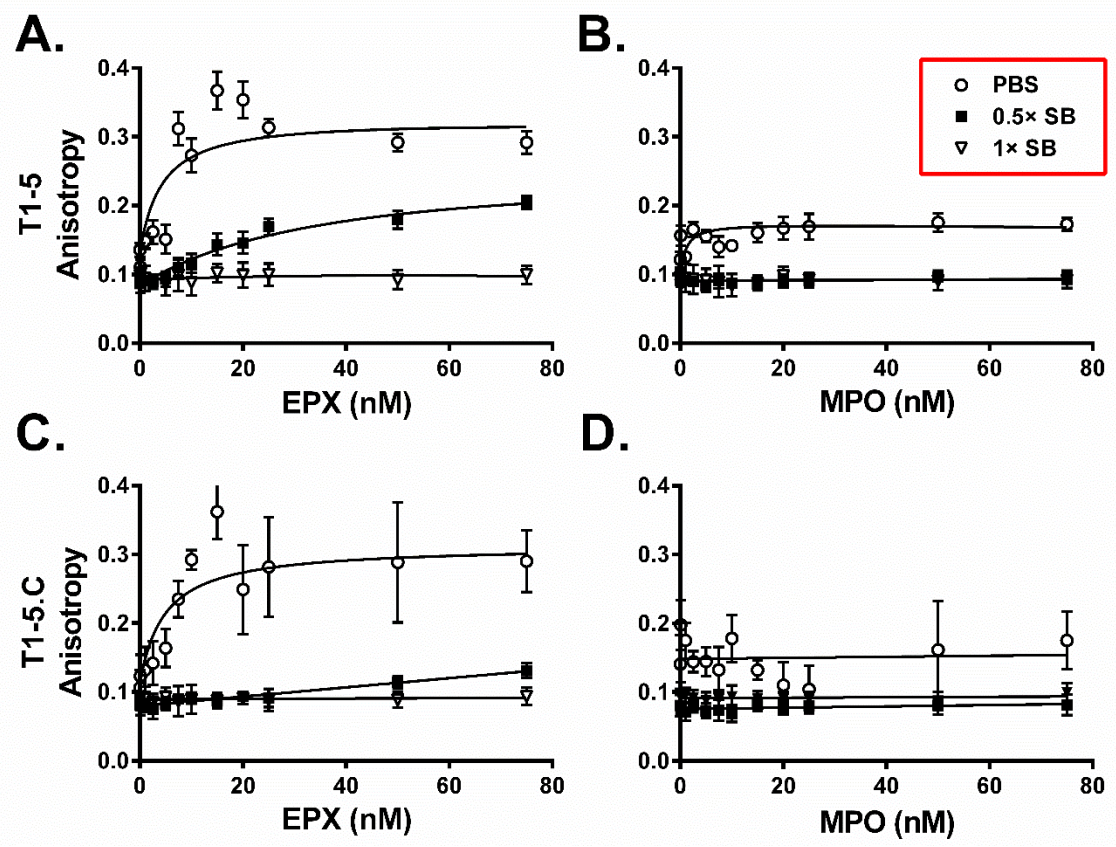

Figure 4.4: Comparing the binding affinity and specificity of the T1-5 and T1-5.C aptamers in various binding buffers. (A) Fluorescence anisotropy of the T1-5 aptamer with EPX and (B) MPO in PBS (white circles), 0.5× SB (black squares), and 1× SB (white triangles). (C) Fluorescence anisotropy using the T1-5.C aptamer with EPX and (D) MPO. Error bars represent the standard deviation of triplicate measurements.

An interesting phenomenon was observed as the T1-5 aptamer experienced reduced fluorescent intensity upon binding EPX (Figure S4.4). To understand this, a small series of tests were set up in parallel. In the first test, different protein targets were mixed with fluorescein-labelled T1-5 and the fluorescent intensity was monitored. The addition of EPX resulted in an

~80% reduction in fluorescent intensity, however no reduction was observed when MPO or BSA were added (Figure S4.4A). This further demonstrates the strong preference of the T1-5 aptamer for EPX over MPO. Next the cause of fluorescent reduction was analyzed by heating up the T1-5/EPX complex in order to unfold the protein (Figure S4.4B). Results show that almost all the fluorescent signal was returned, indicating that the initial loss in signal was due to binding the protein and not likely due to destruction of the fluorophore.

A third test was performed by adding concentrated urea, a denaturant that would strongly disrupt any hydrogen bonding between the nucleobases and EPX (Figure S4.4C). Results show a minimal recovery in fluorescent signal, indicating the aptamer not only binds strongly to EPX, but also likely does so via some hydrophobic π–π stacking interactions with hydrophobic amino acids. The T1-5 aptamer is guanidine-rich, which can form G-quadruplexes strong enough to withstand high amounts of urea.[156] The final test was performed by mixing protein targets with free fluorescein (no DNA aptamer). Results show no change in fluorescent intensity, indicating that the fluorescent reduction is highly dependent on the presence of the DNA aptamer (Figure S4.4D).

These results complicate the fluorescence anisotropy data, as it suggests that the increase in anisotropy may be due in part to the quenching observed. As outlined by the Perrin equation below, reducing the fluorescent lifetime will result in an increased anisotropy (Equation 3). Further characterization using time-correlated single photon counting would provide insight into the type of quenching (static or dynamic), while comparing Stern-Volmer plots at different

temperatures may also be beneficial in identifying the type of quenching.

(3) $$r = \frac{r_0}{1+(\tau/\phi)} \qquad \text{where } \phi = \frac{\eta V}{TR}$$

Equation 3 shows the Perrin equation where r is the observed anisotropy, r_o is the intrinsic anisotropy, τ is the fluorescence lifetime, η is the viscosity, V is the volume of the complex, T is the temperature and R is the ideal gas constant. This does not discredit the anisotropy data, but it does suggest that further characterization is necessary to fully understand this phenomenon.

Finally, we turned our attention towards integrating the aptamer into a simple sensor platform, as illustrated in Figure 4.5A. By utilizing the inherent enzymatic properties of EPX, a pulldown assay was developed and validated using pure EPX in buffer. First, the T1-5 aptamer was biotinylated and immobilized on streptavidin-coated agarose beads. Then, addition of EPX in 0.5× SB allows for the aptamer to selectively sequester EPX from the solution, leaving other off-target proteins free in the supernatant. Washing the beads removes any undesired proteins, leaving only EPX-bound beads remaining. The addition of a peroxidase substrate allows for EPX to convert the tetramethylbenzidine (TMB) substrate into a bright blue signal, clearly detectable by the naked eye. Although this assay could easily be monitored by cellphone imaging software in resource limited areas, we showcase it here using a microwell plate reader for precise quantification.

We first evaluated the sensitivity of the assay using pure EPX in 0.5× SB + 0.01% w/v BSA with concentrations spanning the clinically relevant range of 1 nM – 1 µM (77 ng/mL – 77

μg/mL).[23,38,150] This resulted in a limit of detection (LOD) of 1 nM (blank + 3σ) when using a plate reader, although the naked-eye limit of detection was approximately 25 nM (Figure 4.5B). For comparison, the LOD is quite comparable to a published antibody EPX sensor (circa 6 nM EPX), suggesting it may be sufficient for clinical diagnostic purposes.[150] In addition, the limit of detection for the pull-down assay could theoretically be even lower if combined with an EPX-specific fluorogenic probe.[157]

The specificity of the assay was then assessed by comparing the signal produced by EPX (100 nM) to that of several other granulocytic proteins (at 1 μM). Results showed that despite the high similarity between EPX and several similar peroxidase proteins, the assay only produced signal in the presence of EPX (Figure 4.5C). This was encouraging as EPX and MPO share 70% amino acid sequence identity and 81% sequence similarity according to a protein BLAST search (EPX UniProt #P11678, MPO #P05164).[158] The buffer/BSA controls were included to show that the beads or carrier protein had no impact on colour changes.

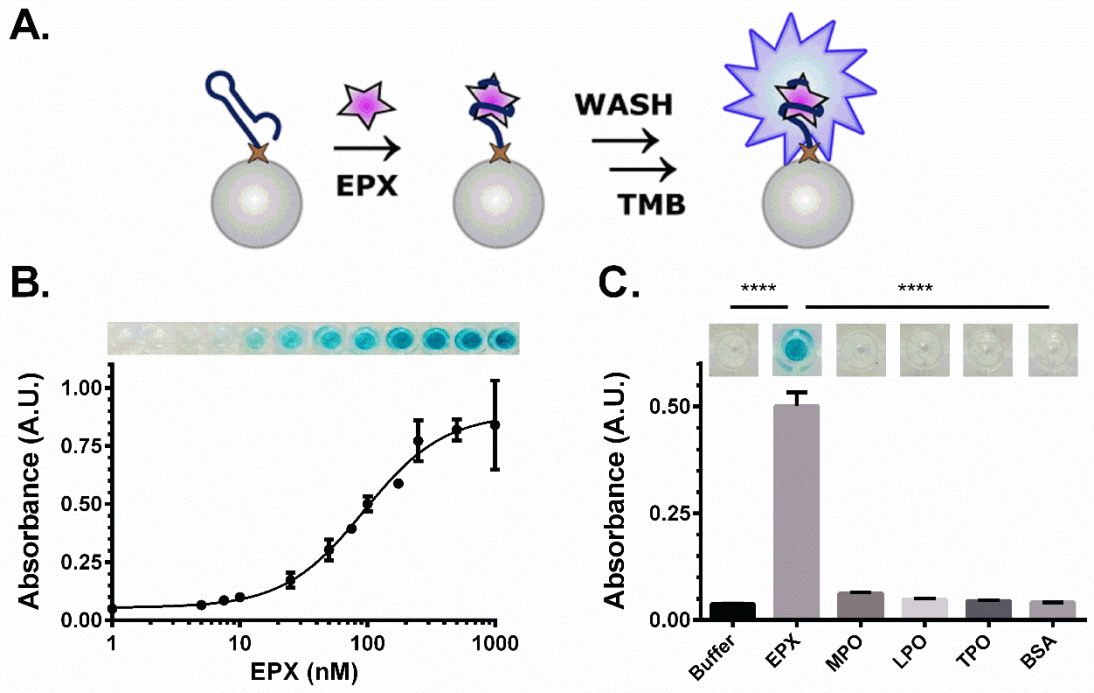

Figure 4.5: EPX pulldown assay. (A) Schematic illustration of the EPX pull-down assay. (B) Sensitivity of the EPX pulldown assay. Image above the graph shows the colour of each well. (C) Specificity of the EPX pulldown assay. Image above the bars shows the colour of each well. Error bars represent the standard deviation of triplicate measurements.

To show the impact of sputum on the assay performance, three healthy sputum samples were each spiked with three different concentrations of EPX and the percent recovery was determined. Results show that the assay was quite successful at the 20 nM and 200 nM EPX concentrations (average of 102% and 87% recovered, respectively) however there was a clear trend with decreasing recovery as EPX concentrations increase. We hypothesize that this may be due to the presence of endogenous DNA/RNA/proteins that hybridize or block the immobilized aptamer, resulting in reduced free aptamers capable of binding EPX. Therefore, when a small concentration of EPX was present, there were sufficient aptamer binding sites to sequester all the free EPX. However, when EPX concentrations increased, there was more EPX than free

aptamers, resulting in some EPX remaining unbound. Overall, this could be overcome by diluting the sputum or increasing the number of beads.

Table 4.1: Recovery of spiked EPX into healthy sputum samples.

Patient	Final spiked [EPX] (nM)	Absorbance	Percent Recovery (%)
A	20	0.147 ± 0.030	104 ± 21
	200	0.577 ± 0.083	86 ± 12
	750	0.681 ± 0.056	81 ± 6
B	20	0.132 ± 0.026	93 ± 18
	200	0.609 ± 0.036	91 ± 5
	750	0.583 ± 0.039	69 ± 5
C	20	0.156 ± 0.036	110 ± 26
	200	0.556 ± 0.101	83 ± 15
	750	0.566 ± 0.054	67 ± 6

4.5 Conclusion

In summary, the first ever DNA aptamer for EPX was discovered using a magnetic bead SELEX method. Despite the challenges of identifying a specific aptamer for an extremely cationic protein, the T1-5 aptamer outlined here possesses both high affinity and great specificity, allowing for the discrimination between MPO and EPX. The aptamer was also integrated into a simple colourimetric assay, with a limit of detection of 1 nM, comparable to the relevant clinical values.[23,38] We believe that this discovery can aid physicians in identifying elevated levels of EPX in sputum, resulting in the potential ability to quickly identify eosinophilic inflammation in asthmatic patients.

Chapter 5 Conclusions and future work

5.1 Summary and future directions

The research in this thesis strived to address the shortcomings of hospital-limited quantitative sputum cytometry by developing alternative diagnostics capable of rapidly quantifying leucocyte biomarkers without the need for specialized technicians. This work began in Chapter 2 with the development of a simple lateral flow test capable of MPO quantification in sputum. While commercial diagnostics already exist for blood MPO, this is the first rapid diagnostic developed for use in sputum. Using a common sandwich immunoassay platform, the device was fabricated in a simple "one and done" format that allowed the user to perform the assay within a single step with results available in 15 minutes. Clinical validation showed the device produced comparable results to the gold standard ELISA. Ultimately, this proved to be a rapid and cost-friendly alternative to quantitative sputum cytometry for identification of neutrophilic bronchitis.

With the success of Chapter 2, Chapter 3 embarked on the goal of developing a similar device for quantification of EPX as a biomarker for eosinophilic bronchitis. Although the device performed well in neat samples, validation experiments determined it was unable to reliably quantify EPX in clinical samples. This was overcome by pretreating samples with protein A/G beads followed by a syringe filtration, restoring proper EPX quantification using the device. With this pretreatment, validation experiments showed the device could differentiate patients

with eosinophilic and neutrophilic bronchitis. This was the first ever rapid diagnostic developed for semi-quantification of EPX in sputum.

Despite this success, the availability of anti-EPX mAbs is extremely limited and costly, while the dynamic range of the assay failed to identify patients with low EPX values. Although the sample pre-treatment greatly improved the device performance, the necessity for sample pre-treatment combined with the cost and LOD limitations sparked the investigation of alternative EPX detection methods shown in Chapter 4. Aptamer selection discovered several anti-EPX aptamer candidates which were then compared via several binding assays, ultimately identifying a single lead aptamer candidate. Utility of the aptamer was demonstrated using a simple pull-down assay, with an order of magnitude lower limit of detection compared to the antibody test from Chapter 3.

While this work has established several new biosensors targeted at exciting clinical opportunities, there is still much to be explored. The next obvious step would be to integrate the new anti-EPX aptamer into a simpler biosensor format than shown in Chapter 4, such as a lateral flow device, alleviating the need for washing steps. This could then be further developed by integrating multiple analyte detection into a single device, allowing for an array of biomarkers to be analyzed at once. The MPO and EPX sensors described in this thesis may lay the groundwork for this, while several other biomarkers pique interest. If DNA/RNA extraction is integrated into the sputum processing steps, then biosensors for quantifying genetic differences between asthma phenotypes would hold tremendous value. Examining mRNA expression of genes *IL1R2* and *NFKB2* can help differentiate eosinophilic and neutrophilic bronchitis, while a small cluster of

genes has been identified as being predictors of corticosteroid response and can even outperform sputum eosinophil counts.[159,160] In cases where neutrophilic bronchitis are suspected, including biomarkers for common bacteria taxa such as *Haemophilus* and *Moraxella* may provide valuable insight on differentiating the inflammatory phenotype and perhaps an effective antibiotic regime.[21]

The large success demonstrated by catalytically active deoxyribozymes for the sensitive and specific detection of pathogens may be an ideal method for combining biorecognition with signal generation. These ribozymes are not only easily integrated into colourimetric detection platforms,[123,161] but they can also be linked to isothermal amplification techniques if additional sensitivity is required.[116,119,162] Overall, it is an exciting time for biosensor research that bridges the gap from the lab bench to clinical utility, allowing more rapid identification of respiratory biomarkers to aid in directing patient therapies.

Appendix I: Chapter 2 Supporting Information

A total of 37 human sputum samples were obtained from volunteers at St. Joseph's Healthcare in Hamilton, ON with their informed consent and approval from the Hamilton Integrated Research Ethics Board. All experiments were performed in compliance with provincial laws and McMaster University guidelines. The samples were from a mix of patients suffering from various breathing difficulties as well as healthy individuals. Sputum collection, preparation, and cell count methods have been described previously.[147] Briefly, sputum is induced in a pulmonary function laboratory through inhalation of normal or hypotonic aerosol saline. A small amount of sputum (typically 0.1–0.3 g) is separated from saliva using an inverted microscope and tweezers, and then diluted 1:1 (v:v) with 0.1% dithiothreitol and 4.5% saline. This mixture is filtered to give a homogenous suspension of cells. A commercial Accufilter device is available for this procedure and provides a detailed protocol summary.[163] Total cell counts are determined by diluting the cell suspension 1:1 with 4% trypan blue and using a hemocytometer. The differential 400-cell counts were obtained from Wright-Giemsa stained cytospins using a Midas III automated cell stainer (EMD Chemicals Inc., NJ, USA). Patient sputum samples were divided into 3 groups based on cell staining results:

Healthy (H). Sputum contains eosinophils at less than 2% of total cells with a total cell count less than 9.7 million cells per gram.

Neutrophilic (N). Sputum contains eosinophils less than 2% of total cells with a total cell count more than 15 million cells per gram and neutrophils greater than 65%. All samples had confirmed bacterial infections, either by standard culture methods or by sequencing of the V3–4 region of the 16S ribosomal RNA gene extracted from sputum whole cell lysate. The most common bacteria isolated were *S. pneumoniae*, *H. influenzae* or Anerobic species such as *Prevotella* and *S. milleri*.

Eosinophilic (E). Sputum contains eosinophils at greater than 3% of total cells with a total cell count less than 10 million cells per gram.

Gold nanoparticles were prepared by reducing gold chloride with 1% sodium citrate using the protocol described by Hayat *et al.*[164] Briefly, 25 mL of 0.01% $HAuCl_4$ solution was boiled, then 0.75 mL of 1% trisodium citrate was added while stirring. As the solution boiled, the colour changed from bright yellow to bright red. At this point, the solution was boiled for an additional 5 minutes. The solution was cooled and then stored at 4 °C until use. Before coupling to antibodies, the AuNP solution pH was adjusted to 9.5 dropwise using K_2CO_3 (0.2 M). Average AuNP size was determined to be 15 nm ± 3 nm *via* TEM imaging (Figure S2.2).

Labelling of anti-MPO antibodies with AuNP was performed in phosphate buffered saline (PBS, 137 mM NaCl, 2.7 mM KCl, 8.1 mM Na_2HPO_4, 1.5 mM KH_2PO_4, pH 7.4). 0.4

μL (3.2 mg/mL, total 1.2 μg) of mouse anti-human-MPO monoclonal antibody (LS-C9174, LifeSpan BioSciences) was added to 18 μL of pH 9.5 AuNPs (~2 nM). The solution was mixed by pipetting and incubated for 45 minutes at room temperature. 2 μL of 10% BSA, pH 7.5 (50–61–00, KPL) was added and incubated another 45 minutes at room temperature. The solution was centrifuged for 60 minutes at 18 000 ×G at 4 °C. The supernatant was removed, and the pellet was resuspended in 25 μL resuspension solution (0.7% w/v sucrose, 0.07% w/v sodium azide in PBS).

Both sample and conjugate pads were prepared by cutting Millipore C083 cellulose sheets (GFCP103000, Millipore) into 0.5 cm × 1 cm strips. The strips were treated with 0.5% v/v Tween 20 and 0.5% w/v HSA (A1653, Sigma) for 30 minutes, then dried 2 hours at 37 °C. 25 μL of the resuspended anti-MPO antibody solution was pipetted onto the conjugate pad, which was then dried for 2 hours at 37 °C before test strip assembly. The test line was prepared by printing 0.24 μL (3.4 mg/mL, total 0.82 μg) of unlabelled mouse anti-human- MPO monoclonal antibody (LS-C9172, LifeSpan BioSciences) onto the designated Test zone on Millipore HF180 nitrocellulose (NC) paper using a Scienion S5 printer (see ESI and Figure S2.3 & S2.4 for more information on printing). A control line was prepared by printing 0.14 μL (2.0 mg/mL, total 0.27 μg) of goat anti-mouse polyclonal antibody (LS-C60700, LifeSpan BioSciences) to the control zone. The NC paper was then blocked for 30 minutes in 1% BSA, and then washed twice for 10 seconds in PBS. Absorbent pads (AP1002500, Millipore) were cut into 0.5 cm × 2 cm strips and the

entire test strip was assembled on a 0.5 cm × 6 cm DCM backing card as shown in Figure S2.1.

The LFT utilizes a standard direct sandwich immunoassay approach (Figure S2.1). Briefly, filtered patient sputum was diluted 1:1 (in PBS with 1% BSA) and added to the sample pad. This sputum then reacts with gold-labelled mouse anti-human-MPO antibodies on the conjugate pad, tagging MPO with the gold-labelled antibodies. As the sputum moves along the test strip by capillary flow, it passes over a defined area (Test Line, T) coated with a different mouse anti-human MPO antibody.

These antibodies bind the AuNP-linked MPO, producing a purple colour. Any unreacted mouse Au-labelled antibodies then pass over an area coated in goat anti-mouse antibodies (Control Line, C). Remaining Au-labelled antibodies are bound, confirming the test functioned properly. Results could be observed in 15 minutes, with samples being imaged at 45 minutes to ensure test completion. The tests were imaged using a handheld scanner (FlipoPal 100C mobile scanner with factory settings) and the colour intensity of the test lines was analyzed using ImageJ software.

To perform the analysis, images were first imported into ImageJ then were inverted. The intensity of the test line was converted to a 256-bit grey scale to produce a quantitative colour intensity where 0 represents a pure white region while 255 represents a pure black region. A blank region of the LFT was also measured to correct for any background signal from the nitrocellulose/AuNPs and subtracted from the test line

intensity. Statistical analysis was performed using a two-tailed unpaired Student's *t*-test with GraphPad Prism 6 software.

A commercial ELISA kit was also used to quantify MPO concentrations in the patient sputum samples. The ELISA followed a traditional indirect sandwich procedure as outlined in the product protocol (DY3174, R&D Systems). Briefly, a microplate was coated with capture antibody (4 μg/mL in PBS, 100 μL) and let sit overnight (23 °C). The next morning the plate was washed by adding wash buffer (WB, 0.05% Tween 20 in PBS, 300 μL), gently shaking, then removing the wash buffer. The wash step was repeated 5 times. The plate was blocked using reagent diluent (RD, 1% BSA in PBS, 300 μL) for one hour (23 °C) then washed. The sputum was added (diluted 1:1000 or 1:5000 in PBS, 100 μL) and allowed to incubate for 1 hour (23 °C). The plate was then washed and detection antibody was added (50 ng mL^{-1} in RD, 100 μL). After 2 hours of incubation, the plate was washed and streptavidin-HRP was added (diluted 1:200 in RD, 100 μL). After 20 min, the plate was washed and H_2O_2 and 3,3′,5,5′-tetramethylbenzidine substrate were added (T4444, Sigma, 100 μL). After a 15 minute reaction, the reaction was quenched using sulfuric acid (0.1 M, 100 μL) and the absorbance was quantified using a Tecan M1000 microplate reader (λ_{abs} = 450 nm). Data was analyzed using Microsoft Excel, Origin 8, and GraphPad Prism 6 software.

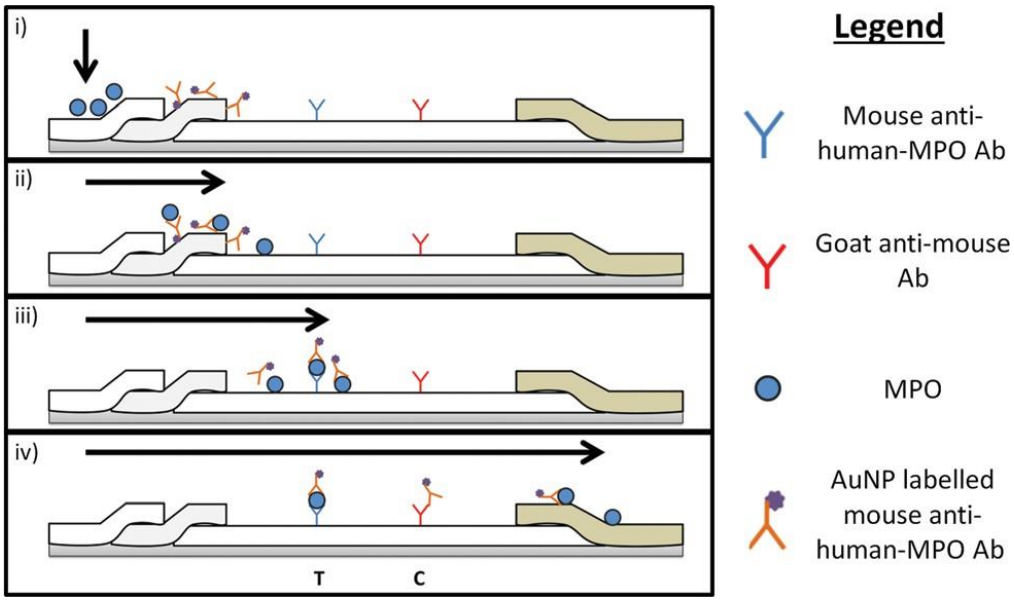

Figure S2.1 General schematic of the MPO LFT Assay. (i) Sputum containing MPO is added to the sample pad. (ii) Capillary flow wicks the sputum down to the conjugate pad where AuNP-tagged mouse anti-human- MPO antibodies bind MPO in the sputum. (iii) A separate anti-MPO antibody printed on the Test line (T) captures the gold-labelled MPO, producing a dark purple line. (iv) Goat anti-mouse antibodies printed on the control line (C) capture excess gold-labelled antibodies to produce a dark purple line, confirming the test functioned properly.

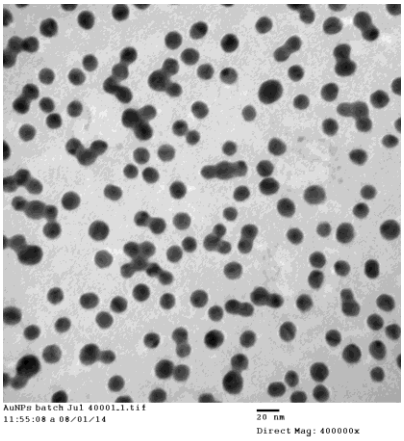

Figure S2.2 Transmission electron microscopy of synthesized AuNPs. Average size is 15 ± 3 nm.

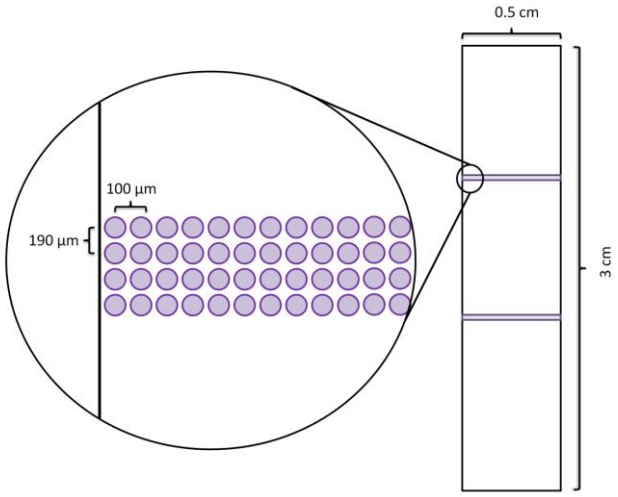

Figure S2.3 Printer layout of the nitrocellulose paper with measurements shown.

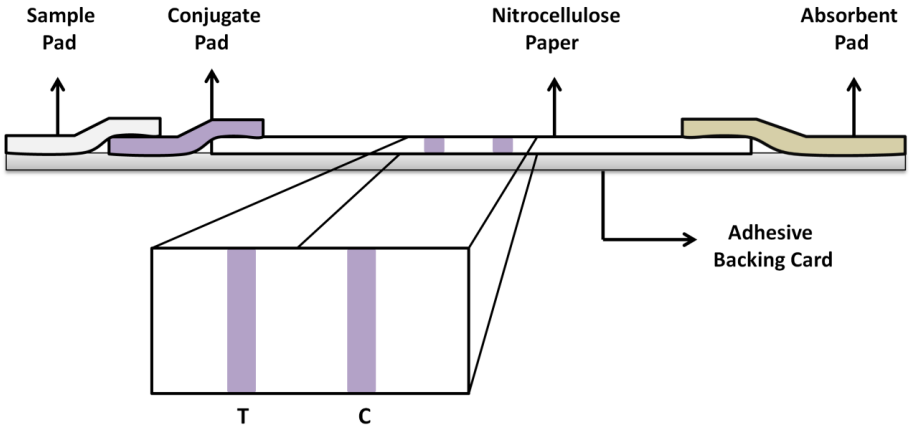

Figure S2.4 Horizontal layout of the immunochromatographic test strip. The enlarged area depicts an aerial view of the Test (T) line and the Control (C) line.

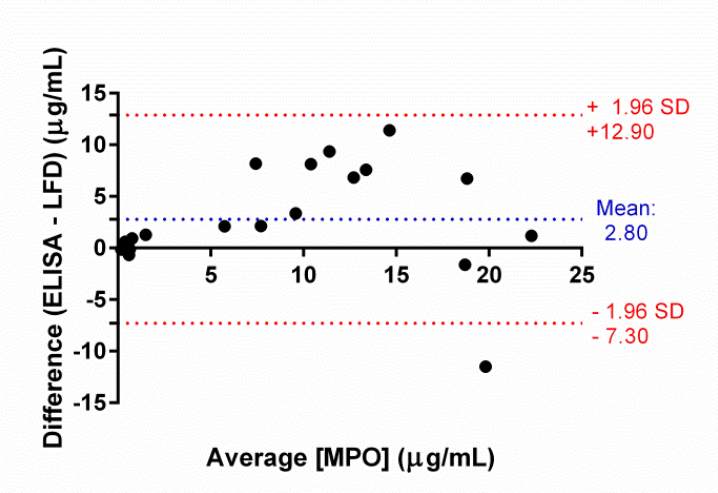

Figure S2.5 Bland-Altman plot assessing the agreement between the developed LFD and a commercial MPO ELISA. A slight bias (2.80 µg/mL) is observed towards the commercial ELISA.

Appendix II: Chapter 3 Supporting Information

Buffers used:

Coating buffer (CB): KPL Product #50-84-01 diluted from 10× to 1× using ddH_2O water.

Blocking buffer (BB): KPL Product #50-61-00 diluted from 10% to 1% using ddH_2O water.

Washing buffer (WB): 2 mM Imidazole, 0.01% Tween 20, pH 7.

ELISA substrate: Alkaline phosphatase chromogen (Abcam, #ab7413)

Washing buffer 2 (WB2): 20 mM Tris-HCl, 500 mM KCl, 0.1% v/v Triton-X, pH 7.4.

PBS: 10 mM Na_2HPO_4, 1.8 mM KH_2PO_4, 2.7 mM KCl, 137 mM NaCl, pH 7.4.

Release agent: 10 mM Tris-HCl, 5% w/v sucrose, 0.5% v/v Tween 20, 0.5% w/v BSA,

Resuspension buffer: 10 mM Tris-HCl, 0.7 % w/v sucrose, 0.07% w/v sodium azide, pH 8

AuNP synthesis and labelling: The methods have been described previously.[165] Briefly, 25 mL of 2.2 mM sodium citrate was refluxed until boiling, then 167 µL of gold chloride (25 mM) was added. This was refluxed for 20 minutes at 100 °C. The temperature was then reduced to 90 °C and an additional 167 µL gold chloride was added for 30 minutes. 9.1 mL of this solution was removed and discarded, then 8.8 mL of ddH_2O was added. Once the solution reached 90 °C, 300 µL of 60 mM sodium citrate was added, followed by 167 µL of gold chloride. This was heated at 90 °C for 30 minutes. Two more additions of gold chloride (167 µL) were added, each being followed by 30 minutes of heating. Once complete, the AuNPs were cooled to room temperature and stored at 4 °C until use. Particle sizes were approximated spectrophotometrically using a common protocol.[166]

Before coupling to antibodies, the AuNP (20 µL per LFT, 0.8 nM) solution was adjusted to a pH of 9 using Na_2CO_3 (0.2 M). Once adjusted, EPX detection antibody (1 µg) was immediately added and mixed for 45 minutes at room temperature. The antibody binds the AuNP via a combination of hydrophobic and electrostatic interactions, hence the necessity to adjust the pH of the AuNP to the pI of the protein (i.e. pH 9). 10% w/v BSA was then added to a final concentration of 1% and mixed an additional 45 minutes. The samples were spun at 14 000 ×G at 4 °C to pellet the conjugates and the supernatant was discarded. The conjugates were resuspended in 25 µL of resuspension buffer and added to sample pads. These pads were then referred to as “conjugate pads”.

Printing EPX LFT: The methods have been described previously.[143] Briefly, the nitrocellulose membrane (HF180, Millipore) was equilibrated at 80% relative humidity for 60 minutes prior to printing using a humidifier in a closed chamber. The test line was printed by

depositing small ~400 pL droplets in a 40×4 XY grid. The droplets were 100 µm apart in the X-direction and 190 µm apart in the Y-direction, eventually forming a narrow 570 µm thick line. Each LFT contained ~1 µg of EPX capture antibody on the test line and 0.25 µg of goat anti-mouse antibody on the control line. After printing, the LFT was dried at room temperature for 30 minutes then blocked in 1% BSA blocking solution (95059-124, VWR) for 30 minutes. After blocking, the LFT was washed 2 × 15 seconds in 1× PBS and dried 2 hours at room temperature prior to test strip assembly.

Sputum collection, processing, and cell staining: The methods have been described previously.[147,167]

Sputum immunoprecipitation[148,168]: Processed sputum samples (100 µL) were mixed with 30 µL of settled IP beads (Pierce Protein A/G Kit, #20421, Thermo Fisher) and PBS (150µL) and mixed one hour at 4°C. The samples were then spun and the supernatant was removed and kept for LFT analysis.

Lateral flow test: The LFT was calibrated using pure EPX in 1× phosphate buffered saline (PBS) and 0.1% w/v bovine serum albumin (BSA). The LFTs were imaged using a Flip-Pal (#100C) handheld scanner 15 minutes after sample addition. Patient samples (100 µL) were tested by adding the samples to the LFT and imaging after 15 minutes.

Immunoprecipitation filtration for fLFT: Similar to the IP protocol, Processed sputum samples (100 µL) were mixed with 30 µL of settled IP beads and 70 µL of PBS for 15 minutes at room temperature. The sample was filtered using a 3 mL syringe (Becton Dickinson, #309657) and 0.22 µm filter disc (Merck Millipore, SLGL0250S), then flushed with 100 µL of PBS. The filter has a void volume of ~150 µL, resulting in a total of 150 µL of processed sputum being recovered.

EPX ELISA: The protocol is similar to what has already been published.[38] Briefly, a microwell plate was pre-coated with an EPX capture antibody (4 µg/mL in CB, 100 µL) and incubated at 4 °C overnight. The plate was washed 5× using washing buffer (WB, 300 µL) then coated with BB for 2 hours. After washing 5× using WB, patient samples were added (50 µL)

and incubated over night at 4 °C. After washing, EPX detection (0.8 µg/mL in 0.5×WB, 100 µL) antibody was added and incubated 60 minutes at room temperature. After washing 5× with WB, streptavidin-alkaline phosphatase (diluted 1:500 in SB, 100 µL) was added for 30 minutes. After washing 5× with WB, ELISA substrate was added (100 µL) and the absorbance was monitored using a TECAN M1000 plate reader (544 nm) for 60 minutes. A calibration curve was created using pure EPX, with a 4PL-standard curve used to quantify the unknown samples.

Anti-EPX-Ig ELISA[148,168]: Well plates were coated with EPX (1 µg/mL, 100 µL) overnight at 4 °C, followed by several washes using WB. Sputum supernatant samples were added (40 µL with 40 µL of 0.1× BB, titer 1:2) at 4 °C overnight, followed by more washing. Samples were probed using biotinylated anti-mouse IgG, with streptavidin-alkaline phosphatase used for colourimetric development.

Data processing: All LFTs were processed in ImageJ similar to our previous work.[143] Briefly, the contrast was adjusted to a minimum value of 63 and max value of 253, then the images were inverted. The intensity of the LFT test line was measured using the "measure" function, and corrected by subtracting background colour. All analysis was performed using Microsoft Excel 2016 and GraphPad Prism 6.01 (La Jolla, CA, USA). Although this software is ideal for quantifying exact line intensities, perhaps this level of analysis in a clinical setting is troublesome as it would require an optical reader to achieve such precise quantification. An alternative would be the use of a reference card to which the line intensities could be compared, which is common in commercial use of lateral flow tests for semi-quantitative analysis.

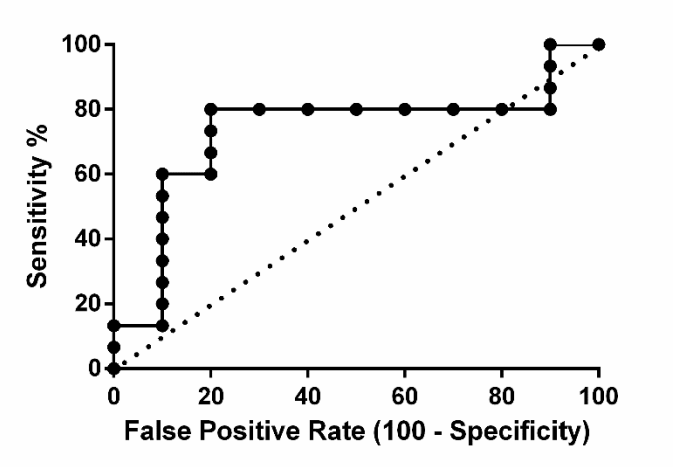

Figure S3.1: receiver operating characteristic curve of the sensitivity and specificity of the fLFT for identifying patients above 3% eosinophils.

Appendix III: Chapter 4 Supporting Information

S4.1. Oligonucleotides and Chemicals: All DNA oligonucleotides (Tables S1, S4) were obtained from Integrated DNA Technologies (Iowa, USA), and purified by standard 10%

dPAGE (7M urea) prior to use. NHS-Activated Magnetic beads (Prod. #88826) and Pierce streptavidin-coated agarose beads (Prod. #20349) were purchased from Thermo Scientific (Burlington, Ontario). Biotools DNA polymerase (#BTL-10043) was purchased from Mandel Scientific (Guelph, Ontario). Eosinophil peroxidase (EPX, #342-60-0.1), Myeloperoxidase (MPO, #426-10-0.1), Thyroid peroxidase (TPO, #ABIN934717) and Lactoperoxidase (LPO, #LS000151) were purchased from Cedarlane (Burlington, Ontario). Enhanced K-blue TMB substrate was from Neogen (#308175, KY, USA). Buffers are outlined in Table S4.2. All other chemicals were purchased from Sigma-Aldrich and used without further purification.

S4.2. Instruments: A Tecan M1000 plate reader was used for microplate fluorescence readings at an excitation wavelength of 490 nm and emission at 520 nm, with the exception of fluorescence anisotropy which was limited to a filter using excitation at 470 nm and emission at 520 nm. PCR was performed using a Dual 48 Bio-Rad thermal cycler. Agarose gels were visualized using a Bio-Rad ChemiDoc imaging system and quantified using Image Lab 6.0 software. Dynamic light scattering (DLS) was performed using a ZEN3600 Zetasizer Nano ZS instrument (Malvern Panalytical, United Kingdom) and a QS quartz Suprasil high precision cuvette (Hellma Analytics, Germany). Pictures of the microwell plates used in the EPX pulldown assay were taken using a LG G5 cellular phone operated in automatic mode, then adjusted using Microsoft Photos to increase the colour and brightness 20%. Figures were made using GraphPad Prism 5 or Excel 2016 software.

S4.3. Conjugating EPX/MPO to magnetic beads: Proteins were coupled to the magnetic beads (MBs) as per the manufacturer's protocol. Briefly summarized, 300 µL of MBs

were mixed with Cwb A for 15 seconds, then placed in a magnetic stand to collect the beads and discard the supernatant. EPX (for positive selection) or MPO (for counter selection) was then added and mixed on a 360° microfuge tube rotator for two hours at room temperature. The MBs were collected with a magnetic stand and the supernatant was saved for quantification of unbound protein via Bradford assay. The MBs were washed with Cwb B for 15 seconds, then the supernatant was discarded. This was repeated for a total of two washes with Cwb B, followed by two washes with ddH_2O. Qb was then added for two hours to quench any unreacted amide moieties, followed by three washes with ddH_2O. The beads were suspended in Sb and kept at 4 °C until use.

S4.4. *In vitro* aptamer selection: The selection protocol was loosely based around two previous protocols and is outlined in Figure 4.1.[169,170] Two types of selections were performed in parallel: one using a traditional aptamer selection (T1) and a second that contained a hairpin DNA oligo (DNA_B) as a blocking DNA strand to compete with the DNA_L for EPX binding (T2). Both EPX-coated MBs and MPO-coated MBs were washed 5× using 1× WB prior to use. The first round of selection began by denaturing the DNA_L (50 µL in 1× SB, 1 nmol total DNA) at 90 °C for 5 minutes then cooling at room temperature for 20 minutes. Counter selection was performed by mixing the DNA_L with MPO-coated MBs (diluted to 500 µL in 1× SB, 50 pmol of MPO) for 30 minutes at room temperature, then partitioning the beads using a magnetic stand. The supernatant was removed and added to a solution of EPX-coated MBs (diluted to 500 µL in 1× SB, 50 pmol of EPX) for 2 hours. After binding was complete, the beads were washed 9× using 1× WB (500 µL each). Each wash supernatant from the first round was kept and

concentrated using standard ethanol precipitation. The wash efficiency was analyzed by performing the PCR on each wash supernatant and monitored by gel electrophoresis, as seen in Figure S4.1. Nine washes were required to ensure all weak binding sequences were removed. After washing, the bound aptamers were eluted from the beads by adding EB (300 µL) and heating at 80 °C for 40 minutes. The supernatants were then precipitated by standard ethanol precipitation and resuspended with 50 µL of ddH_2O.

The PCR protocol was based on work previously from our group and requires two PCR stages (PCR1 and PCR2).[171] The PCR1 mixture (50 µL) contained 1 µL of the eluted DNA along with 1 µM FP1, 1 µM RP1, 200 mM dNTPs, 1× PCR reaction buffer (75 mM Tris-HCl, 2 mM $MgCl_2$, 50 mM KCl, 20 mM $(NH_4)_2SO_4$, pH 9), and 2.5 U Biotools DNA polymerase. Thermal cycles were performed as follows: 95 °C for 60 seconds; ~15-18 cycles of 90 °C for 45 seconds, 53 °C for 45 seconds, 70 °C for 45 seconds. PCR progress was monitored by agarose gel electrophoresis (2% w/v containing 1× SYBR GOLD) to ensure sufficient PCR product. PCR2 was performed to fluorescently label the aptamer strand and differentiate it from the antisense strand. Using 1 µL of the PCR1 product as a template, PCR2 was performed with primers FP2 and RP2 instead of FP1 and RP1 for 15 rounds following the same protocol as PCR1. The triethylene glycol spacer in RP2 prevents the amplification of the poly-A region of RP2, resulting in the aptamer sequence being 20 nucleotides shorter than the antisense strand. The aptamer was purified using dPAGE and used as the library for the next round of selection. After 15 rounds of selection the enriched library was PCR amplified and sent for deep sequencing. The values used for each round of selection can be found below in Table S3.

S4.5. Electrophoretic mobility shift assay (EMSA): The EPX binding of all 10 aptamer candidates (Table S4.4) were analyzed using the EMSA. Binding reactions were performed in 10 µL of 1× SB containing 3 nM fluorescently labelled DNA, 1 ng poly(dI-dC) and target protein (concentrations ranging from 0 – 100 nM). The T2 aptamers also contained 100 nM DNA_B. After binding for 60 minutes, 10 µL of native loading buffer (1× SB + 40 % w/v sucrose) was added and the samples were loaded into a 0.3 % w/v agarose gel.

S4.6. Dynamic light scattering measurements: The T1-5 aptamer was diluted to a final concentration of 500 nM in 1×SB (40 µL total volume) with or without 0.02% v/v Tween 20. EPX was added to positive samples to a final concentration of 500 nM. All samples were spun at 14 000 ×G for 5 minutes to remove any large particles such as dust. To test the impact of electrical current on the stability of the EPX/DNA complex, the entire 40 µL mixture was transferred into a 0.5 mL microfuge tube and set into an agarose gel stand and run for 15 minutes, then remeasured using the Zetasizer Nano ZS instrument.

S4.7. Anisotropy of DNA/protein interactions: Fluorescence anisotropy was performed in 50 µL reactions containing 3 nM DNA in buffer (PBS, 0.5× SB, or 1× SB) and protein (EPX or MPO) ranging from 0 – 100 nM. A G-factor of 1.105 was determined by calibrating the fluorimeter with 1 nM fluorescein in 10 mM NaOH, and used to correct for the polarization bias of the system. All samples were prepared in duplicate, then measured in triplicate after reacting for 60 minutes at room temperature.

S4.8. EPX pulldown assay: Streptavidin-coated agarose beads (2 µL of slurry per replicate, typically 60-120 µL per batch) were first washed 3× using 100 µL 0.5× SB. BioT1-5

(50 pmol per replicate, typically 3 nmol – 6 nmol total) was diluted in 0.5×SB and heated at 90 °C for 5 minutes, then cooled to room temperature for 20 minutes. Once cool, the DNA was mixed with the agarose beads for 60 minutes on a 360° microfuge tube rotator for 60 minutes at room temperature. Once complete, the beads were washed with 5× 100 µL of 0.5× SB + 0.01% w/v BSA. The beads were resuspended to 10 µL and aliquoted for each reaction. Unused beads were stored at 4 °C until use.

For binding reactions, 10 µL of conjugated beads were mixed with 10 µL of EPX (in 0.5× SB + 0.01% w/v BSA) for 30 minutes, then washed 3× using 100 µL 0.5× SB. Beads were resuspended to 10 µL in 0.5× SB and mixed with 40 µL of Neogen Enhanced K-blue substrate, and absorbance at 660 nm was taken after 15 minutes.

To test EPX recovery with sputum, 30 µL of EPX was mixed with 10 µL of sputum (final EPX concentration of 20 nM, 200 nM or 750 nM), then added to 10 µL of conjugated beads for 30 minutes. Samples were washed and tested as described above.

Table S4.1: Sequences of DNA oligonucleotide used in the DNA aptamer selections.

Name	Description	Sequence (5' – 3')
$DNA_L SS$	DNA Library	ATGCCATCCTACCAACN$_{15}$GATTCAGACCTTACGN$_{25}$GAGCTCTGAACTCG
BiotinSS	Immobilized $DNA_L SS$	/5BiosG/TACCGCAAAAAAAAAACGTAAGGTCTGAATC
DNA_L	DNA Library	ATGCCATCCT ACCAACN$_{40}$GAGCTCTGAACTGG
FP1	Forward primer 1	ATGCCATCCT ACCAAC
FP2	FAM Forward primer 2	/56-FAM/ATGCCATCCT ACCAAC
RP1	Reverse primer 1	CCAGTTCAGA GCTC

RP2	Poly-A Reverse primer 2		AAAAAAAAAA AAAAAAAAAA/isp9/CCAGTTCAGA GCTC
DNA_B	Hairpin (blocker DNA)		GCGGCCCATT CTTCATTTTA GGGCCGC
T1-5.A	Truncated T1-5		/56-FAM/CCATCCTACCAACCAGGGGGACAGTGCAAAGGGGTAGGGAG
T1-5.B	Truncated T1-5		/56-FAM/ATGCCATCCTACCAATAGGGAGGGGGCTAGGGGGGAGCTCTGAACTCG
T1-5.C	Truncated T1-5		/56-FAM/ATGCCATCCTACCAACCAGGGGGACAGTGCAAAGGGAGCTCTGAACTCG
T1-5.D	Mutated T1-5		/56-FAM/ATGCCATCCTACCAACCAGAAAGACAGTGCAAAGAAATAGAAAGAGAGCTAGAAGAAAGCTCTGAACTCG
BioT1-5	Biotin T1-5		ATGCCATCCTACCAACCAGGGGGACAGTGCAAAGGGGTAGGGAGGGGGCTAGGGGGGAGCTCTGAACTCGTTTTTTTTTTT/3BIO/

Table S4.2: Buffers used in this work.

Name	Description	Contents
1× SB	Selection buffer	50 mM Tris, 1 M NaCl, 5 mM $MgCl_2$, 2 mM KCl, 0.01 % v/v Tween 20, pH 9
1× WB	Wash buffer	50 mM Tris, 1 M NaCl, 5 mM $MgCl_2$, 2 mM KCl, 0.1 % v/v Tween 20, pH 9
EB	Elution buffer	50 mM Tris, 4 M guanidine thiocyanate, 1 mM DTT, pH 9
Cwb A	Coupling wash buffer A	1 mM Ice-cold HCl
Cwb B	Coupling wash buffer B	0.1 M glycine, pH 2
Cb	Coupling buffer	50 mM borate, pH 8.5
Qb	Quenching buffer	3 M ethanolamine, pH 9
Sb	Storage buffer	Coupling buffer + 0.05% w/v NaN_3

Table S4.3: SELEX outline for the T1 and T2 selections including times and values used. T1 selection was performed without the blocker oligo, while the T2 selection was performed with the blocker oligo.

Round	**DNA library, pmol**	**Beads, pmol**	**Positive selection time, minutes**	**Counter selection, minutes**	**Blocker DNA, pmol (blocker:target)**
1	1000	1×10^7 beads, 50	120	30	500 (10:1)
2	~ 50	1×10^6 beads, 5	60		50 (10:1)
3		1×10^6 beads, 5	60	30	50 (10:1)
4		1×10^6 beads, 5	30		100 (20:1)

5		1×10^5 beads, 0.5	30	30	10 (20:1)
6		1×10^5 beads, 0.5	15		10 (20:1)
7		1×10^5 beads, 0.5	15	30	20 (40:1)
8		1×10^4 beads, 0.05	15		2 (40:1)
9		1×10^4 beads, 0.05	15	30	2 (40:1)
10		1×10^4 beads, 0.05	10		2 (40:1)
11		1×10^4 beads, 0.05	10	30	4 (80:1)
12		1×10^4 beads, 0.05	10		4 (80:1)
13		1×10^4 beads, 0.05	5	30	8 (160:1)
14		1×10^4 beads, 0.05	5		8 (160:1)
15		1×10^4 beads, 0.05	5	30	8 (160:1)

Table S4.4: High-throughput sequencing results from round 15 for target EPX.

Name	Sequence (5' → 3)	Multiplicity	Percent
T1-1	/56-FAM/ATGCCATCCTACCAACCACGGGGATCGGGTGGGGGCTAGGCGGCGTGTGCACGGGGGAGCTCTGAACTCG	30702	7.40
T1-5	/56-FAM/ATGCCATCCTACCAACCAGGGGGACAGTGCAAAGGGGTAGGGAGGGGGCTAGGGGGGAGCTCTGAACTCG	1888	0.45
T1-8	/56-FAM/ATGCCATCCTACCAACCAGTTGCCGGTGGGGGTGACCCGGTGGGGGAGGGTGTGGGGGAGCTCTGAACTCG	1342	0.32
T1-15	/56-FAM/ATGCCATCCTACCAACCGGGGGAGCAAGGTGTAGGGGTAGGGGGCCATGCGAGGGGGAGCTCTGAACTCG	999	0.24
T1-20	/56-FAM/ATGCCATCCTACCAACAGCAGCGGGCGGGGGCCAGTGGGGGATGTAGCCGGGGGTGGAGCTCTGAACTCG	686	0.17
T2-1	/56-FAM/ATGCCATCCTACCAACCGCGGGAGGAGACTGGTGTAGGGGGCATGGGATGGCCTGGGAGCTCTGAACTCG	48472	4.28
T2-9	/56-FAM/ATGCCATCCTACCAACACGACCGGTGTAGAGGGGGGTATACGGAATGGGGGTTGTGGAGCTCTGAACTCG	6923	0.61
T2-10	/56-FAM/ATGCCATCCTACCAACAGGGAGGGGGCGGTTAGGGAATGGTGGTCCGGGCGGGGTAGAGCTCTGAACTCG	6191	0.55
T2-18	/56-FAM/ATGCCATCCTACCAACATGGGGATATCCGGCGGGGGCATCAGGGGGGAGTGCGGGTGAGCTCTGAACTCG	3958	0.35
T2-40	/56-FAM/ATGCCATCCTACCAACCAGGGGGCGCGGGAGGGGGCCTGACGTCGAGGGGGTTGGGGAGCTCTGAACTCG	2171	0.19

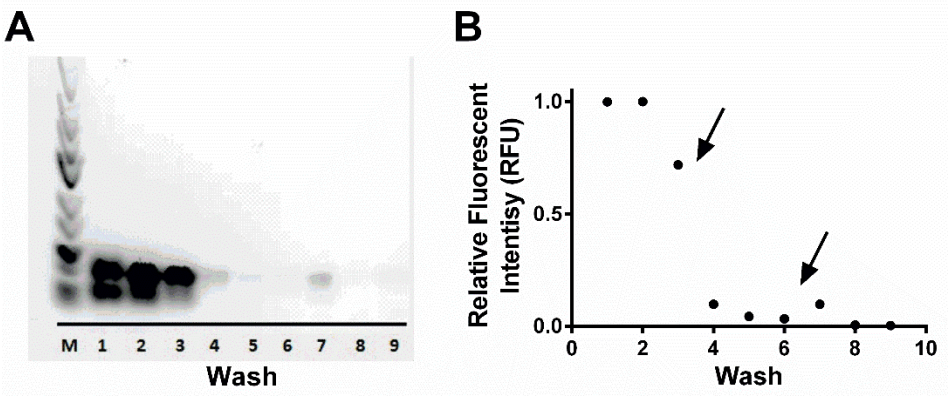

Figure S4.1: PCR analysis of wash supernatants during positive selection. (A) Agarose gel

image of PCR amplified supernatants from various wash cycles. “M” indicates a DNA ladder marker, while the numbers correspond to the wash cycle. (B) Quantified intensity of PCR products. Arrows indicate when the sample was moved to a fresh microcentrifuge tube.

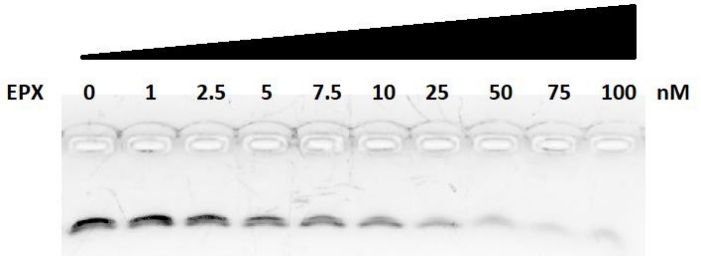

Figure S4.2: Agarose gel image of T1-5 aptamer (3 nM) with increasing amounts of EPX.

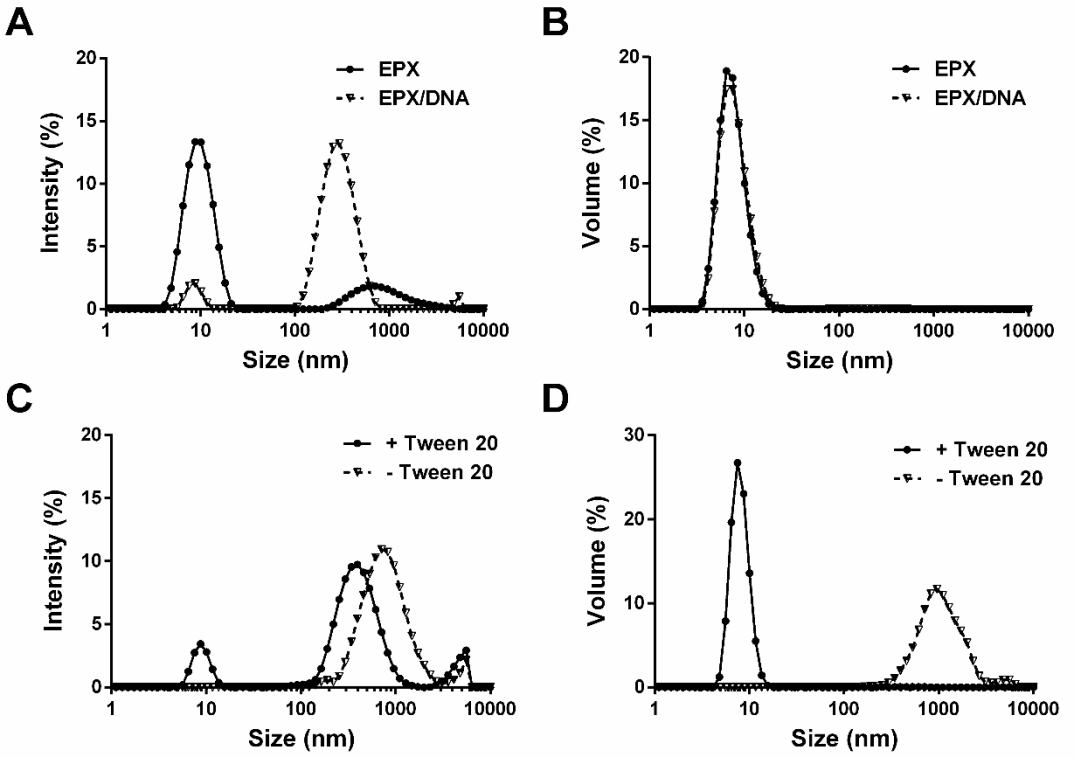

Figure S4.3: Dynamic light scattering analysis of the EPX-aptamer complex. Each trace represents an average of three measurements. (A) Intensity of scattered light and (B) volume calculation for EPX and a 1:1 EPX:DNA mixture. The impact of electrical current can be seen with and without a surfactant present, as shown by the (C) intensity and (D) volume calculation.

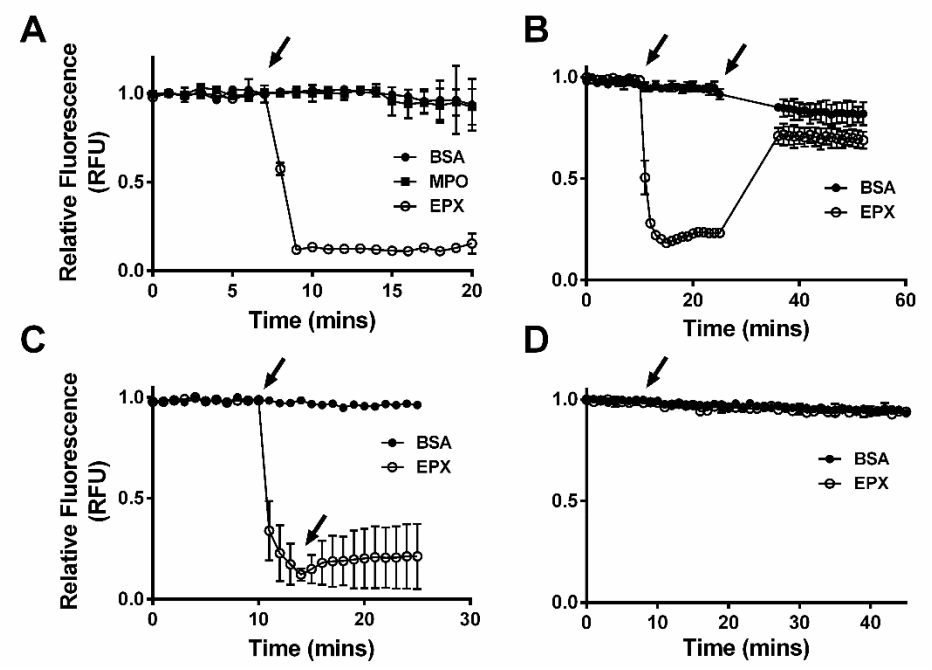

Figure S4.4: Examining the fluorescent reduction observed when the T1-5 DNA aptamer binds to EPX. The first arrow in all images indicates when protein was added. (A) Comparing the fluorescent intensity when various proteins are added. (B) Fluorescent recovery caused by heating the DNA mixture. The second arrow indicates when the sample was removed and heated at 90 °C. (C) Fluorescent recovery caused by denaturing the DNA-protein complex with 1M urea. The second arrow indicates when urea was added. (D) Fluorescent quenching observed between free fluorescein (no aptamer) and protein.

References

(1) Global Asthma Network. *Glob. Asthma Rep.* **2014**, *5* (3).

(2) Theriault, L.; Hermus, G.; Goldfarb, D.; Stonebridge, C.; Bounajm, F. *Conf. Board Canada* **2012**.

(3) *Am J Respir Crit Care Med* **2000**, *162*, 2341–2351.

(4) Chung, K. F.; Wenzel, S. E.; Brozek, J. L.; Bush, A.; Castro, M.; Peter, J.; Adcock, I. M.; Bateman, E. D.; Bel, E. H.; Bleecker, E. R.; Sterk, P. J.; Adcock, I. M.; Bateman, E. D.; Bel, E. H.; Bleecker, E. R.; Boulet, L. *Eur Respir J* **2013**, *43*, 1–112.

(5) Katial, R. K.; Bensch, G. W.; Busse, W. W.; Chipps, B. E.; Denson, J. L. *J ALLERGY CLIN IMMUNOL Pr.* **2017**, *5* (2), S1–S14.

(6) Jayaram, L.; Pizzichini, M. M.; Cook, R. J.; Boulet, L. P.; Lemière, C.; Pizzichini, E.; Cartier, A.; Hussack, P.; Goldsmith, C. H.; Laviolette, M.; Parameswaran, K.; Hargreave, F. E. *Eur. Respir. J.* **2006**, *27* (3), 483–494.

(7) Green, R. H.; Brightling, C. E.; McKenna, S.; Hargadon, B.; Parker, D.; Bradding, P.; Wardlaw, A. J.; Pavord, I. D. *Lancet* **2002**, *360*, 1715–1721.

(8) Siva, R.; Green, R. H.; Brightling, C. E.; Shelley, M.; Hargadon, B.; McKenna, S.; Monteiro, W.; Berry, M.; Parker, D.; Wardlaw, A. J.; Pavord, I. D. *Eur. Respir. J.* **2007**, *29* (5), 906–913.

(9) Dasgupta, A.; Neighbour, H.; Nair, P. *Pharmacol. Ther.* **2013**, *140* (3), 213–222.

(10) Svenningsen, S.; Nair, P. *Front. Med.* **2017**, *4* (158).

(11) Lim, H. F.; Nair, P. *Can Respir J* **2013**, *20* (6), 415–417.

(12) *NIH Natl. Hear. Lung, Blood Inst.* **2007**.

(13) Miller, M. R.; Hankinson, J.; Brusasco, V.; Burgos, F.; Casaburi, R. *Eur. Respir. J.* **2005**, *26* (2), 319–338.

(14) Bateman, E. D.; Hurd, S. S.; Barnes, P. J.; Bousquet, J.; Drazen, J. M.; Fitzgerald, M. *Eur Respir J* **2008**, *31*, 143–178.

(15) Reddel, H. K.; Bateman, E. D.; Becker, A.; Boulet, L.; Cruz, A. A.; Drazen, J. M.; Haahtela, T.; Hurd, S. S.; Inoue, H.; Jongste, J. C. De; Jr, R. F. L.; Levy, M. L.; Byrne, P. M. O.; Paggiaro, P.; Pedersen, S. E. *Eur Respir J* **2015**, *46*, 622–639.

(16) Simpson, J. L.; Scott, R.; Boyle, M. J.; Gibson, P. G. *respirology* **2006**, *11*, 54–61.

(17) Gibson, P. G. *Clin Respir J* **2009**, *3*, 198–206.

(18) Mckinley, L.; Alcorn, J. F.; Peterson, A.; Dupont, R. B.; Kapadia, S.; Logar, A.; Henry, A.; Irvin, C. G.; Piganelli, J. D.; Ray, A.; Kolls, J. K. *J. Immunol* **2008**, *181*, 4089–4097.

(19) Ito, K.; Herbert, C.; Siegle, J. S.; Vuppusetty, C.; Hansbro, N.; Thomas, P. S.; Foster, P. S.; Barnes, P. J.; Kumar, R. K. *Am. J. Respir. Cell Mol. Biol.* **2008**, *39* (5), 543–550.

(20) Pelaia, G.; Vatrella, A.; Busceti, M. T.; Gallelli, L.; Calabrese, C.; Terracciano, R.; Maselli, R. *Mediat. Inflamm.* **2015**, *2015* (879783).

(21) Taylor, S. L.; Leong, L. E. X.; Choo, J. M.; Wesselingh, S.; Yang, I. A.; Upham, J. W.; Reynolds, P. N.; Hodge, S.; James, A. L.; Jenkins, C.; Peters, M. J.; Baraket, M.; Marks, G. B.; Gibson, P. G.; Simpson, J. L.; Rogers, G. B. *J. Allergy Clin. Immunol.* **2018**, *141* (1), 94-103.e15.

(22) Corrigan, C. J.; Kay, A. B. *Immunol. Today* **1992**, *13* (12), 501–507.

(23) Nair, P.; Ochkur, S. I.; Protheroe, C.; Radford, K.; Efthimiadis, A.; Lee, N. A.; Lee, J. J. *Allergy Eur. J. Allergy Clin. Immunol.* **2013**, *68* (9), 1177–1184.

(24) Busse, W.; Chupp, G.; Nagase, H.; Albers, F. C.; Doyle, S.; Shen, Q.; Bratton, D. J.; Gunsoy, N. B. *J. Allergy Clin. Immunol.* **2019**, *143* (1), 190–200.

(25) Farne, H. A.; Wilson, A.; Powell, C.; Bax, L.; Milan, S. *Cochrane Database Syst Rev* **2017**, No. 9, 1–124.

(26) Wenzel, S. E. *Lancet* **2006**, *368*, 804–813.

(27) Belda, J.; Leigh, R.; Parameswaran, K.; O'Byrne, P. M.; Sears, M. R.; Hargreave, F. E. *Am. J. Respir. Crit. Care Med.* **2000**, *161* (8), 475–478.

(28) Aziz-Ur-Rehman, A.; Dasgupta, A.; Kjarsgaard, M.; Hargreave, F. E.; Nair, P. *Allergy, Asthma Clin. Immunol.* **2017**, *13* (1), 1–7.

(29) Muniz, V. S.; Weller, P. F.; Neves, J. S. *J Leukoc Biol* **2012**, *92* (August), 281–288.

(30) Walsh, G. M. *Curr Opin Hematol* **2001**, *8*, 28–33.

(31) Acharya, K. R.; Ackerman, S. J. *J Biol Chem* **2014**, *289* (25), 17406–17415.

(32) Trulson, A.; Byström, J.; Engström, A.; Larsson, R.; Venge, P. *Clin Exp Allergy* **2007**, *37*, 208–218.

(33) Abu-Ghazaleh, R.; Dunnette, S.; Loegering, D.; Checkel, J.; Kita, H.; Thomas, L.; Gleichti, J. *J Leukoc Biol* **1992**, *52* (December), 611–618.

(34) Wang, Z.; Yang, J.; Gui, L. *Int. J. Electrochem. Sci.* **2017**, *12*, 9502–9511.

(35) Youn, H.; Her, J.; Mok, J.; Kil, B.; Kim, E.; Park, H.; Ban, C. *Electroanalysis* **2018**, *30* (11), 2597–2603.

(36) Reimert, C. M.; Venge, P. *J. Immunol. Methods* **1991**, *138*, 285–290.

(37) Morioka, J.; Kurosawa, M.; Inamura, H.; Nakagami, R.; Shibata, M. *Int Arch Allergy Immunol* **2000**, *122*, 49–57.

(38) Ochkur, S. I.; Kim, J. D.; Protheroe, C. A.; Colbert, D.; Condjella, R. M.; Bersoux, S.; Helmers, R. A.; Moqbel, R.; Lacy, P.; Kelly, E.

A.; Jarjour, N. N.; Kern, R.; Peters, A.; Schleimer, R. P.; Furuta, G. T.; Nair, P.; Lee, J. J.; Lee, N. A. *J. Immunol. Methods* **2012**, *384* (1–2), 10–20.

(39) Borregaard, N.; Sørensen, O. E.; Theilgaard-mo, K. *Trends Immunol* **2007**, *28* (8), 340–345.

(40) Agner, K. *Acta Chem. Scand.* **1941**, *8*, 1– 62.

(41) Schultz, J.; Shmukler, H. W. *Biochemistry* **1964**, *3* (9), 1234–1238.

(42) Ndrepepa, G. *Clin. Chim. Acta* **2019**, *493* (February), 36–51.

(43) Korkmaz, B.; Moreau, T.; Gauthier, F. *Biochimie* **2008**, *90*, 227–242.

(44) Brinkmann, V.; Reichard, U.; Goosmann, C.; Fauler, B.; Uhlemann, Y.; Weiss, D. S.; Weinrauch, Y.; Zychlinsky, A. *Science (80-.).* **2004**, *303*, 1532–1535.

(45) Burg, D.; Scho, J. P. R.; Brandsma, J.; Staykova, D.; Folisi, C.; Bansal, A.; Nicholas, B.; Xian, Y.; Rowe, A.; Cor, J.; Wilson, S.; Ward, J.; Lutter, R.; Fleming, L.; Shaw, D. E.; Bakke, P. S.; Caruso, M.; Dahlen, S.; Fowler, S. J.; Hashimoto, S.; Horva, I.; Krug, N.; Montuschi, P.; Sanak, M.; Sandstro, T.; Singer, F.; Sun, K.; Pandis, I.; Au, C.; Sousa, A. R.; Adcock, I. M.; Chung, K. F.; Sterk, P. J.; Djukanovic, R.; Skipp, P. J. *J. Proteome Res.* **2018**, *17*, 2072–2091.

(46) Vashist, S. K. *Anal. Biochem.* **2014**, *446* (1), 96–101.

(47) Zhai, L.; Wang, T.; Kang, K.; Zhao, Y.; Shrotriya, P.; Nilsen-Hamilton, M. *Anal. Chem.* **2012**, *84* (20), 8763–8770.

(48) Gibson, P. G.; Simpson, J. L.; Saltos, N. *Chest* **2001**, *119* (5), 1329–1336.

(49) Chavakis, T.; Bierhaus, A.; Al-Fakhri, N.; Schneider, D.; Witte, S.; Linn, T.; Nagashima, M.; Morser, J.; Arnold, B.; Preissner, K. T.; Nawroth, P. P. *J. Exp. Med.* **2003**, *198* (10), 1507–1515.

(50) Hasmann, A.; Gewessler, U.; Hulla, E.; Schneider, K. P.; Binder, B.; Francesko, A.; Tzanov, T.; Schintler, M.; Van der Palen, J.; Guebitz, G. M.; Wehrschuetz-Sigl, E. *Exp. Dermatol.* **2011**, *20* (6), 508–513.

(51) Qureshi, A.; Gurbuz, Y.; Niazi, J. H. *Sensors Actuators, B Chem.* **2012**, *171–172*, 62–76.

(52) Newman, J. D.; Turner, A. P. F. *Biosens. Bioelectron.* **2005**, *20* (12), 2435–2453.

(53) Turner, A. P. F. *Chem. Soc. Rev.* **2013**, *42* (8), 3184.

(54) Velasco-Garcia, M. N. *Semin. Cell Dev. Biol.* **2009**, *20* (1), 27–33.

(55) Van Dorst, B.; Mehta, J.; Bekaert, K.; Rouah-Martin, E.; De Coen, W.; Dubruel, P.; Blust, R.; Robbens, J. *Biosens. Bioelectron.* **2010**, *26* (4), 1178–1194.

(56) Hu, J.; Wang, S.; Wang, L.; Li, F.; Pingguan-Murphy, B.; Lu, T. J.; Xu, F. *Biosens. Bioelectron.* **2014**, *54*, 585–597.

(57) Hossain, S. M. Z.; Brennan, J. D. *Anal. Chem.* **2011**, *83*, 8772–8778.

(58) Hossain, S. M. Z.; Luckham, R. E.; McFadden, M. J.; Brennan, J. D. *Anal. Chem.* **2009**, *81* (21), 9055–9064.

(59) Zakir Hossain, S. M.; Luckham, R. E.; Smith, A. M.; Lebert, J. M.; Davies, L. M.; Pelton, R. H.; Filipe, C. D. M.; Brennan, J. D. *Anal. Chem.* **2009**, *81* (13), 5474–5483.

(60) Hossain, S. M. Z.; Ozimok, C.; Sicard, C.; Aguirre, S. D.; Ali, M. M.; Li, Y.; Brennan, J. D. *Anal. Bioanal. Chem.* **2012**, *403* (6), 1567–1576.

(61) Yager, P.; Floriano, P. N.; Mcdevitt, J. *IEEE Pulse* **2013**, *2* (6), 40–50.

(62) Hoa, X. D.; Kirk, A. G.; Tabrizian, M. *Biosens. Bioelectron.* **2007**, *23* (2), 151–160.

(63) Clark, L. C.; Lyons, C. *Ann. N. Y. Acad. Sci.* **1962**, *102* (1), 29–45.

(64) Clark, L. C. *Int. Anesth. Clin.* **1987**, *25* (3), 1–29.

(65) Updike, S.; Hicks, G. *Nature* **1967**, *214*, 986–988.

(66) Guilbault, G. G.; Montalvo, J. G. *J. Am. Chem. Soc.* **1969**, *91* (8), 2164–2165.

(67) Palchetti, I.; Mascini, M.; Chimica, D.; Lastruccia, V. *Springer Netherlands* **2010**, *54* (February), 15–23.

(68) Wang, J. *Chem. Rev.* **2007**, *108* (2), 814–825.

(69) Comer, J. P. *Anal. Chem.* **1956**, *28* (8), 1748–1750.

(70) Pelton, R. *TrAC - Trends Anal. Chem.* **2009**, *28* (8), 925–942.

(71) Espy, H. H. *TAPPI J.* **1995**, *78* (4), 90–99.

(72) Mark, H. *Cellul. Chem. Technol.* **1980**, *80* (14), 569–581.

(73) Gunasingham, H.; Teo, P. Y. T.; Lai, Y. H.; Tan, S. G. *Biosensors* **1989**, *4* (1), 349–359.

(74) Pasquini, D.; Teixeira, E. de M.; Curvelo, A. A. da S.; Belgacem, M. N.; Dufresne, A. *Compos. Sci. Technol.* **2008**, *68* (1), 193–201.

(75) Incani, V.; Danumah, C.; Boluk, Y. *Cellulose* **2013**, *20* (1), 191–200.

(76) Vuoti, S.; Laatikainen, E.; Heikkinen, H.; Johansson, L. S.; Saharinen, E.; Retulainen, E. *Carbohydr. Polym.* **2013**, *96* (2), 549–559.

(77) Lutz, B. R.; Trinh, P.; Ball, C.; Fu, E.; Yager, P. *Lab Chip* **2011**, *11* (24), 4274.

(78) Fenton, E. M.; Mascarenas, M. R.; López, G. P.; Sibbett, S. S. *ACS Appl. Mater. Interfaces* **2009**, *1* (1), 124–129.

(79) Lutz, B.; Liang, T.; Fu, E.; Ramachandran, S.; Kauffman, P.; Yager, P. *Lab Chip* **2013**, *13* (14), 2840–2847.

(80) Fu, E.; Kauffman, P.; Lutz, B.; Yager, P. *Sensors Actuators, B Chem.* **2010**, *149* (1), 325–328.

(81) Lafleur, L.; Stevens, D.; McKenzie, K.; Ramachandran, S.; Spicar-Mihalic, P.; Singhal, M.; Arjyal, A.; Osborn, J.; Kauffman, P.; Yager, P.; Lutz, B. *Lab Chip* **2012**, *12*, 1119.

(82) Millipore: Considerations for product development. *Rapid lateral flow test strips: considerations for product development*; 2008.

(83) Byrne, B.; Stack, E.; Gilmartin, N.; O'Kennedy, R. *Sensors* **2009**, *9* (6), 4407–4445.

(84) Saper, C. B. *J. Histochem. Cytochem.* **2009**, *57* (1), 1–5.

(85) Stave, J. W.; Lindpaintner, K. *J Immunol* **2013**, *191* (3), 1428–1435.

(86) Wang, J.; Yiu, B.; Obermeyer, J.; Filipe, C. D. M.; Brennan, J. D.; Pelton, R. *Biomacromolecules* **2012**, *13* (2), 559–564.

(87) Stark, B. C.; Kole, R.; Bowman, E. J.; Altman, S. *Proc. Natl. Acad. Sci. U. S. A.* **1978**, *75* (8), 3717–3721.

(88) Kruger, K.; Grabowski, P. J.; Zaug, A. J.; Sands, J.; Gottschling, D. E.; Cech, T. R. *Cell* **1982**, *31* (1), 147–157.

(89) Wilson, D. S.; Szostak, J. W. *Annu. Rev. Biochem.* **1999**, *68*, 611–647.

(90) Ellington, A. D.; Szostak, J. W. *Nature* **1990**, *346*, 818–822.

(91) Robertson, D. L.; Joyce, G. F. *Nature* **1990**, *344*, 467–468.

(92) Tuerk, C.; Gold, L. *Science.* **1990**, *249*, 505–510.

(93) Hermann, T.; Patel, D. J. *Science (80-.).* **2000**, *287* (5454), 820–825.

(94) Tombelli, S.; Minunni, M.; Mascini, M. *Biosens. Bioelectron.* **2005**, *20* (12), 2424–2434.

(95) Jenison, R. D.; Gill, S. C.; Pardi, A.; Polisky, B. *Science (80-.).* **1994**, *263* (5152), 1425–1429.

(96) Chen, A.; Yang, S. *Biosens. Bioelectron.* **2015**, *71*, 230–242.

(97) Xu, H.; Mao, X.; Zeng, Q.; Wang, S.; Kawde, A.; Liu, G.; Xu, H.; Mao, X.; Zeng, Q.; Wang, S.; Kawde, A. *Anal. Chem.* **2009**, *81* (2), 669–675.

(98) Shen, G.; Zhang, S.; Hu, X. *Clin. Biochem.* **2013**, *46* (16–17), 1734–1738.

(99) Liu, J.; Mazumdar, D.; Lu, Y. *Angew. Chemie - Int. Ed.* **2006**, *45* (47), 7955–7959.

(100) MarketResearch. *http://www.marketresearch.com/* **2013**.

(101) Stoltenburg, R.; Reinemann, C.; Strehlitz, B. *Anal Bioanal Chem* **2005**, *383*, 83–91.

(102) Bock, L. C.; Griffin, L. C.; Latham, J. a; Vermaas, E. H.; Toole, J. J. *Nature* **1992**, *355* (6360), 564–566.

(103) Chandra, S.; Gopinath, B. **2007**, 171–182.

(104) Wang, T.; Chen, C.; Larcher, L. M.; Barrero, R. A.; Veedu, R. N. *Biotechnol. Adv.* **2019**, *37* (1), 28–50.

(105) Bayat, P.; Nosrati, R.; Alibolandi, M.; Rafatpanah, H.; Abnous, K.; Khedri, M.; Ramezani, M. *Biochimie* **2018**, *154*, 132–155.

(106) Martin, J. A.; Mirau, P. A.; Chushak, Y.; Chávez, J. L.; Naik, R. R.; Hagen, J. A.; Kelley-loughnane, N. *Anal. methods* **2015**.

(107) Arnold, S.; Pampalakis, G.; Kantiotou, K.; Silva, D.; Cortez, C.; Missailidis, S.; Sotiropoulou, G. *Biol. Chem.* **2012**, *393* (May), 343–353.

(108) McKeague, M.; McConnell, E. M.; Cruz-Toledo, J.; Bernard, E. D.; Pach, A.; Mastronardi, E.; Zhang, X.; Beking, M.; Francis, T.; Giamberardino, A.; Cabecinha, A.; Ruscito, A.; Aranda-Rodriguez, R.; Dumontier, M.; DeRosa, M. C. *J. Mol. Evol.* **2015**, *81* (5–6), 150–161.

(109) Cowperthwaite, M. C.; Ellington, A. D. *J. Mol. Evol.* **2008**, *67*, 95–102.

(110) Gold, L.; Ayers, D.; Bertino, J.; Bock, C.; Bock, A. *PLoS One* **2010**, *5* (12).

(111) Girotti, S.; Eremin, S.; Montoya, A.; Moreno, M. J. **2010**, 687–695.

(112) Wichers, J.; Abad-somovilla, A.; Sua, C.; Amerongen, A. Van; Abad-fuentes, A. *Biosens. Bioelectron.* **2013**, *42*, 170–176.

(113) Nardo, F. Di; Alladio, E.; Cavalera, S.; Giovannoli, C.; Spano, G.; Anfossi, L.; Di, F.; Alladio, E.; Baggiani, C.; Giovannoli, C.; Spano, G.; Anfossi, L. *Talanta* **2018**.

(114) Su, S.; Nutiu, R.; Filipe, C. D. M.; Li, Y.; Pelton, R.; Uni, V.; West, M. S.; Ls, O.; April, R. V. **2007**, No. 1, 1300–1302.

(115) Carrasquilla, C.; Little, J. R. L.; Li, Y.; Brennan, J. D. *Chem. Eur. J.* **2015**, *21* (20), 7369–7373.

(116) Hsieh, P. Y.; Monsur Ali, M.; Tram, K.; Jahanshahi-Anbuhi, S.; Brown, C. L.; Brennan, J. D.; Filipe, C. D. M.; Li, Y. *ChemBioChem*

2017, *18* (6), 502–505.

(117) Ali, M. M.; Brown, C. L.; Jahanshahi-Anbuhi, S.; Kannan, B.; Li, Y.; Filipe, C. D. M.; Brennan, J. D. *Sci. Rep.* **2017**, *7* (1), 1–10.

(118) Hui, C. Y.; Liu, M.; Li, Y.; Brennan, J. D. *Angew. Chem. Int. Ed.* **2018**, *130*, 4639–4643.

(119) Liu, M.; Hui, C. Y.; Zhang, Q.; Gu, J.; Kannan, B.; Jahanshahi-Anbuhi, S.; Filipe, C. D. M.; Brennan, J. D.; Li, Y. *Angew. Chemie - Int. Ed.* **2016**, *128* (8), 2759–2763.

(120) Toley, B. J.; Covelli, I.; Belousov, Y.; Ramachandran, S.; Kline, E.; Scarr, N.; Vermeulen, N.; Mahoney, W.; Lutz, B. R.; Yager, P. *Analyst* **2015**, *140* (April 2016), 7540–7549.

(121) Liu, M.; Zhang, Q.; Kannan, B.; Botton, G.; Yang, J.; Soleymani, L.; Brennan, J.; Li, Y. *Angew. Chemie Int. Ed.* **2018**, *130*, 12620–12623.

(122) Connelly, J. T.; Rolland, J. P.; Whitesides, G. M. *Anal. Chem.* **2015**, *87* (15), 7595–7601.

(123) Ali, M. M.; Wolfe, M.; Tram, K.; Gu, J.; Filipe, C.; Li, Y.; Brennan, J. D. *Angew. Chem. Int. Ed.* **2019**, *58* (29), 9907–9911.

(124) Zhang, H.; Xu, Y.; Fohlerova, Z.; Chang, H.; Iliescu, C.; Neuzil, P. *Trends Anal. Chem.* **2019**.

(125) Dong, T.; Wang, G. A.; Li, F. *Anal Bioanal Chem* **2019**, 1–14.

(126) Dweik, R. A.; Boggs, P. B.; Erzurum, S. C.; Irvin, C. G.; Leigh, M. W.; Lundberg, J. O.; Olin, A.; Plummer, A. L.; Taylor, D. R. *Am J Respir Crit Care Med* **2011**, *184*, 602–615.

(127) Wagener, A. H.; Nijs, S. B. De; Lutter, R.; Sousa, A. R.; Weersink, E. J. M.; Bel, E. H.; Sterk, P. J. *Thorax* **2015**, *70*, 115–120.

(128) Nair, P.; Kjarsgaard, M.; Armstrong, S.; Efthimiadis, A.; O'Byrne, P. M.; Hargreave, F. E. *J. Allergy Clin. Immunol.* **2010**, *126* (2), 404–406.

(129) Nair, P. *Can. Respir. J* **2013**, *20* (2), 117–120.

(130) Bizeto, L.; Mazzolini, A. B.; Ribeiro, M.; Stelmach, R.; Cukier, A.; Nunes, M. P. T. *Brazilian J. Med. Biol. Res.* **2008**, *41* (8), 193–198.

(131) Röpcke, S.; Holz, O.; Lauer, G.; Müller, M.; Rittinghausen, S.; Ernst, P.; Lahu, G.; Elmlinger, M.; Krug, N.; Hohlfeld, J. M. *PLoS One* **2012**, *7* (10), 1–11.

(132) Martinez, A. W.; Phillips, S. T.; Whitesides, G. M.; Carrilho, E. *Anal. Chem.* **2010**, *82* (1), 3–10.

(133) Kannan, B.; Jahanshahi-Anbuhi, S.; Pelton, R. H.; Li, Y.; Filipe, C. D. M.; Brennan, J. D. *Anal. Chem.* **2015**, *87* (18), 9288–9293.

(134) Vella, S. J.; Beattie, P.; Cademartiri, R.; Laromaine, A.; Martinez, A. W.; Phillips, S. T.; Mirica, K. A.; Whitesides, G. M. *Anal. Chem.* **2012**, *84* (6), 2883–2891.

(135) Liu, G.; Mao, X.; Phillips, J. A.; Xu, H.; Tan, W.; Zeng, L. *Anal. Chem.* **2009**, *81* (24), 10013–10018.

(136) Elain, F.; Liang, T.; Spicar-Mihalic, P.; Houghtaling, J.; Ramachandran, S.; Yager, P. *Anal. Chem.* **2012**, *10* (84), 4574–4579.

(137) Thornton, C. R. *Clin. Vaccine Immunol.* **2008**, *15* (7), 1095–1105.

(138) McDonnell, B.; Hearty, S.; Finlay, W. J. J.; O'Kennedy, R. *Anal. Biochem.* **2011**, *410* (1), 1–6.

(139) Offermann, N.; Conrad, K.; Fritzler, M. J.; Fooke Achterrath, M. *J. Immunol. Methods* **2014**, *403* (1–2), 1–6.

(140) Barczyk, A.; Sozanska, E.; Trzaska, M.; Pierzchala, W. *Chest* **2004**, *126* (2), 389.

(141) Metso, T.; Venge, P.; Haahtela, T.; Peterson, C. G. B.; Sevéus, L. *Thorax* **2002**, *57*, 449–451.

(142) Keatings, V. M.; Barnes, P. J. *Am. J. Respir. Crit. Care Med.* **1997**, *155*, 449–453.

(143) Wolfe, M. G.; Zhang, Q.; Hui, C.; Radford, K.; Nair, P.; Brennan, J. D. *Analyst* **2016**, *141* (23), 6438–6443.

(144) Nair, P.; Zhang, Q.; Brennan, J. D. *J. Asthma* **2014**, *0903*, 1–8.

(145) Posthuma-Trumpie, G. A.; Korf, J.; Van Amerongen, A. *Anal. Bioanal. Chem.* **2009**, *393* (2), 569–582.

(146) O'Farrell, B. In *Lateral Flow Immunoassay*; Wong, R. C., Tse, H. Y., Eds.; Humana Press, New York, 2009; pp 1–33.

(147) Nair, P.; Hargreave, F. E. *Chest* **2010**, *138* (2), 38S-43S.

(148) Mukherjee, M.; Bulir, D. C.; Radford, K.; Kjarsgaard, M.; Huang, C. M.; Jacobsen, E. A.; Ochkur, S. I.; Catuneanu, A.; Lamothe-Kipnes, H.; Mahony, J.; Lee, J. J.; Lacy, P.; Nair, P. K. *J. Allergy Clin. Immunol.* **2018**, *141* (4), 1269–1279.

(149) Wardlaw, A. J.; Brightling, C. E.; Green, R.; Woltmann, G.; Bradding, P.; Pavord, I. D. *Clin Sci* **2002**, *103* (2), 201–211.

(150) Wolfe, M. G.; Mukherjee, M.; Radford, K.; Brennan, J. D.; Nair, P. *Allergy* **2018**, *74* (6), 1176–1178.

(151) Nutiu, R.; Li, Y. *Angew. Chem. Int. Ed.* **2005**, *44*, 1061–1065.

(152) Tucker, W. O.; Shum, K. T.; Tanner, J. A. *Curr. Pharm. Des.* **2012**, *18* (14), 2014–2026.

(153) Narayanan, J.; Xiong, J. Y.; Liu, X. Y. *J. Phys. Conf. Ser.* **2006**, *28* (1), 83–86.

(154) Gatto, B.; Palumbo, M.; Sissi, C. *Curr. Med. Chem.* **2009**, 1248–1265.

(155) Zuker, M. *Nucleic Acids Res.* **2003**, *31* (13), 3406–3415.

(156) Zhang, W.; Liu, M.; Lee, C.; Salena, B. J.; Li, Y. *Sci. Rep.* **2018**, *8* (1), 3–10.

(157) Kim, T. Il; Hwang, B.; Lee, B.; Bae, J.; Kim, Y. *J. Am. Chem. Soc.* **2018**, *140* (37), 11771–11776.

(158) Altschul, S. F.; Madden, T. L.; Schäffer, A. A.; Zhang, J.; Zhang, Z.; Miller, W.; Lipman, D. J. **1997**, *25* (17), 3389–3402.

(159) Baines, K. J.; Hons, B.; Simpson, J. L.; Wood, L. G. *J Allergy Clin Immunol* **2011**, *127* (1), 153-160.e9.

(160) Baines, K. J.; Simpson, J. L.; Wood, L. G.; Scott, R. J.; Fibbens, N. L.; Powell, H.; Cowan, D. C.; Taylor, D. R.; Cowan, J. O.; Gibson, P. G. *J Allergy Clin Immunol* **2014**, *133* (4), 997–1007.

(161) Ali, M. M.; Li, Y. *Angew. Chem.* **2009**, *2* (5), 1–5.

(162) Liu, M.; Zhang, Q.; Chang, D.; Gu, J.; Brennan, J. D.; Li, Y. *Angew. Chem. Int. Ed.* **2017**, *56* (22), 6142–6146.

(163) Chaboillez, S.; Dasgupta, A.; Prince, P.; Boulet, L. P.; Lemière, C. *Can. Respir. J.* **2013**, *20* (4), 248–252.

(164) Hayat, M. A. *Colloidal gold: principles, methods, and applications*; Academic Press, 1989; Vol. 1.

(165) Bastús, N. G.; Comenge, J.; Puntes, V. *Langmuir* **2011**, *27* (17), 11098–11105.

(166) Haiss, W.; Thanh, N. T. K. .; Aveyard, J.; Fernig, D. G. *Anal. Chem.* **2007**, *79* (11), 4215–4221.

(167) Pizzichini E, Pizzichini MMM, Efthimiadis A.; Evans S, Morris MM, Squillace, D, Gleich, GJ, Dolovich, J, Hargreave, F. *Am. J. Respir Crit Care Med* **1996**, *154*, 308–317.

(168) Mukherjee, M.; Lim, H. F.; Thomas, S.; Miller, D.; Kjarsgaard, M.; Tan, B.; Sehmi, R.; Khalidi, N.; Nair, P. *Allergy, Asthma Clin. Immunol.* **2017**, *13* (1).

(169) Bruno, J. G. *Biochem. Biophys. Res. Commun* **1997**, *234* (1), 117–120.

(170) Duan, N.; Wu, S.; Chen, X.; Huang, Y.; Xia, Y.; Ma, X.; Wang, Z. *J. Agric. Food Chem* **2013**, *61*, 3229–3234.

(171) Ali, M. M.; Aguirre, S. D.; Lazim, H.; Li, Y. *Angew. Chemie Int. Ed.* **2011**, *50* (16), 3751–3754.